



**NAVAL
POSTGRADUATE
SCHOOL**

MONTEREY, CALIFORNIA

THESIS

**WIND TURBINE POWER GENERATION EMULATION
VIA DOUBLY FED INDUCTION GENERATOR CONTROL**

by

Gregory W. Edwards

December 2009

Thesis Advisor:
Second Reader:

Alexander L. Julian
Roberto Cristi

Approved for public release; distribution is unlimited

REPORT DOCUMENTATION PAGE			Form Approved OMB No. 0704-0188	
Public reporting burden for this collection of information is estimated to average 1 hour per response, including the time for reviewing instruction, searching existing data sources, gathering and maintaining the data needed, and completing and reviewing the collection of information. Send comments regarding this burden estimate or any other aspect of this collection of information, including suggestions for reducing this burden, to Washington headquarters Services, Directorate for Information Operations and Reports, 1215 Jefferson Davis Highway, Suite 1204, Arlington, VA 22202-4302, and to the Office of Management and Budget, Paperwork Reduction Project (0704-0188) Washington DC 20503.				
1. AGENCY USE ONLY (Leave blank)		2. REPORT DATE December 2009	3. REPORT TYPE AND DATES COVERED Master's Thesis	
4. TITLE AND SUBTITLE Wind Turbine Power Generation Emulation Via Doubly Fed Induction Generator Control			5. FUNDING NUMBERS	
6. AUTHOR(S) Gregory W. Edwards				
7. PERFORMING ORGANIZATION NAME(S) AND ADDRESS(ES) Naval Postgraduate School Monterey, CA 93943-5000			8. PERFORMING ORGANIZATION REPORT NUMBER	
9. SPONSORING /MONITORING AGENCY NAME(S) AND ADDRESS(ES) N/A			10. SPONSORING/MONITORING AGENCY REPORT NUMBER	
11. SUPPLEMENTARY NOTES The views expressed in this thesis are those of the author and do not reflect the official policy or position of the Department of Defense or the U.S. Government.				
12a. DISTRIBUTION / AVAILABILITY STATEMENT Approved for public release; distribution is unlimited			12b. DISTRIBUTION CODE	
13. ABSTRACT (maximum 200 words) In this thesis, we emulate a Wind Turbine Generator by driving a Doubly Fed Induction Generator (DFIG) via a DC motor with variable input torque capability. The two circuits of concern are the DFIG and Supply-side circuits. They are electrically coupled with back-to-back Space Vector Modulators (SVMs) that are coupled through a DC Link consisting of a capacitor bank. The SVMs, with DC Link, provide bi-directional power flow between the DFIG rotor and Supply-side power supply. The Supply-side circuit senses voltage, current and DC Link voltage (V_{DC}), and sends the sensed inputs to a Field Programmable Gate Array (FPGA), which is used to derive control of V_{DC} so that it is maintained at 200V via SVM. The DFIG circuit senses rotor current, stator voltage, rotor speed, and rotor electrical position, which are used to derive a current reference that is used to control the rotor speed using a Proportional Integral Controller (PI). For our application we show that the DFIG rotor speed can be controlled (subsynchronous, synchronous, or supersynchronous) for a given input torque and thus distributes the power generated by the DFIG as predicted between the rotor and stator.				
14. SUBJECT TERMS Double Fed Induction Generator (DFIG), Space Vector Modulation (SVM), Wind Turbine, Field Programmable Gate Array (FPGA), Bi-directional Power Flow			15. NUMBER OF PAGES 101	
			16. PRICE CODE	
17. SECURITY CLASSIFICATION OF REPORT Unclassified	18. SECURITY CLASSIFICATION OF THIS PAGE Unclassified	19. SECURITY CLASSIFICATION OF ABSTRACT Unclassified	20. LIMITATION OF ABSTRACT UU	

THIS PAGE INTENTIONALLY LEFT BLANK

Approved for public release; distribution will be unlimited

**WIND TURBINE POWER GENERATION EMULATION VIA DOUBLY FED
INDUCTION GENERATOR CONTROL**

Gregory W. Edwards
Lieutenant, United States Navy
B.S., Texas A&M University, 2003

Submitted in partial fulfillment of the
requirements for the degree of

MASTER OF SCIENCE IN ELECTRICAL ENGINEERING

from the

**NAVAL POSTGRADUATE SCHOOL
December 2009**

Author: Gregory W. Edwards

Approved by: Alexander L. Julian
Thesis Advisor

Roberto Cristi
Second Reader

Jeffrey B. Knorr
Chairman, Department of Electrical and Computer Engineering

THIS PAGE INTENTIONALLY LEFT BLANK

ABSTRACT

In this thesis, we emulate a Wind Turbine Generator by driving a Doubly Fed Induction Generator (DFIG) via a DC motor with variable input torque capability. The two circuits of concern are the DFIG and Supply-side circuits. They are electrically coupled with back-to-back Space Vector Modulators (SVMs) that are coupled through a DC Link consisting of a capacitor bank. The SVMs, with DC Link, provide bi-directional power flow between the DFIG rotor and Supply-side power supply.

The Supply-side circuit senses voltage, current and DC Link voltage (VDC), and sends the sensed inputs to a Field Programmable Gate Array (FPGA), which is used to derive control of VDC so that it is maintained at 200V via SVM.

The DFIG circuit senses rotor current, stator voltage, rotor speed, and rotor electrical position, which are used to derive a current reference that is used to control the rotor speed using a Proportional Integral Controller (PI). For our application we show that the DFIG rotor speed can be controlled (subsynchronous, synchronous, or supersynchronous) for a given input torque and thus distributes the power generated by the DFIG as predicted between the rotor and stator.

THIS PAGE INTENTIONALLY LEFT BLANK

TABLE OF CONTENTS

I.	INTRODUCTION.....	1
	A. MISSION	1
	B. OBJECTIVE	1
	C. APPROACH.....	2
	D. THESIS ORGANIZATION.....	4
II.	DFIG THEORY	5
	A. INDUCTION MACHINE EQUATIONS	5
	B. SYSTEM CONFIGURATION	10
III.	CONTROLLER SCHEME.....	15
	A. CONTROLLER COMPONENTS	15
	B. SUPPLY-SIDE CONTROLLER.....	15
	C. DFIG-SIDE CONTROLLER	20
	D. SPACE VECTOR MODULATION.....	22
	E. ENCODER IMPLEMENTATION	26
IV.	RESULTS	31
	A. OVERVIEW.....	31
	B. SUPPLY-SIDE EXPERIMENTS	31
	C. DFIG-SIDE EXPERIMENTS.....	33
V.	CONCLUSIONS AND FUTURE RESEARCH.....	45
	A. CONCLUSIONS	45
	B. FUTURE RESEARCH.....	45
APPENDIX A:	DATASHEETS.....	47
APPENDIX B:	MATLAB M-FILES	53
	A. MATLAB INITIAL CONDITIONS FILE	53
	B. MATLAB M-FILE USED FOR SPACE VECTOR MODUALTION.....	56
	C. MATLAB M-FILES FOR CHIPSCOPE INTERFACE.....	58
APPENDIX C:	SIMULINK/ XILINX MODEL OF WIND TURBINE GENERATOR SYSTEM (DFIG-SIDE).....	61
APPENDIX D:	SIMULINK/ XILINX MODEL OF WIND TURBINE GENERATOR SYSTEM (SUPPLY-SIDE)	69
APPENDIX E:	TRANSFORMATIONS	73
	LIST OF REFERENCES.....	75
	INITIAL DISTRIBUTION LIST	77

THIS PAGE INTENTIONALLY LEFT BLANK

LIST OF FIGURES

Simplified Circuit of Wind Turbine DFIG System.....	xvii
Simulation: Input Torque Transient Showing Rotor Power Reversal.	xviii
Experimental: Rotor Current and Voltage with Power Flow from the Rotor.....	xix
Experimental: Rotor Current and Voltage with Power Flow to the Rotor.	xx
Figure 1. Simplified Circuit of Wind Turbine DFIG System.....	3
Figure 2. Simplified Single Phase Circuit Showing the Inductor Connections.	11
Figure 3. Simulink Model of Supply-side Voltage Angle Calculation.	17
Figure 4. Inner and Outer PI Control Loops for the Supply-side Controller.	20
Figure 5. Simulink Model of DFIG-side Slip Angle Calculation.	21
Figure 6. SIMULINK DFIG Controller Topology.....	22
Figure 7. SEMISTACK-IGBTs and SVM Hexagon [From 8].	23
Figure 8. SVM Digital Implementation Diagram [From 8].	25
Figure 9. Experimental: Encoder A, B and Z Pulse Configuration.....	26
Figure 10. Architecture Used to Derive Rotor Angular Position from the Encoder.	27
Figure 11. Experimental: Calibrated Rotor Electrical Angular Position.....	29
Figure 12. Simulation: Supply-side Voltage and Current with i_{d_ref} at 2A and -2A.	32
Figure 13. Experimental: Supply-side Voltage and Current with i_{d_ref} at 2A and -2A.	33
Figure 14. Simplified Circuit of Wind Turbine DFIG System.....	34
Figure 15. Simulation: DFIG-side Voltage and Current with i_{d_ref} at 2A and -2A.	36
Figure 16. Experimental: DFIG-side Voltage and Current with i_{d_ref} at 2A and -2A.	37
Figure 17. Simulation: Input Torque Transient Showing Rotor Power Reversal.	38
Figure 18. Experimental: Rotor Current and Voltage with Power Flow from the Rotor.	39
Figure 19. Experimental: Rotor Current and Voltage with Power Flow to the Rotor.	40
Figure 20. Simulation: Increase in Rotor Speed with a Constant Input Torque.	41
Figure 21. Experimental: Rotor Current and Voltage While Subsynchronous.....	42
Figure 22. Experimental: Rotor Current and Voltage While Synchronous.	43
Figure 23. Experimental: Rotor Current and Voltage While Supersynchronous.....	44

THIS PAGE INTENTIONALLY LEFT BLANK

LIST OF TABLES

Table 1. Space Vector Modulation Switching Pattern [From 9].....25
Table 2. Encoder Truth Table with Directed Actions.28

THIS PAGE INTENTIONALLY LEFT BLANK

LIST OF ABBREVIATIONS AND ACRONYMS

BNC	Bayonette Neil-Concelamn connector
DFIG	Doubly Fed Induction Generator
FPGA	Field Programmable Gate Array
IGBT	Insulated Gate Bipolar Transistor
ISE	Integrated Software Environment
MTL	Microtech Laboratory Inc.
PI	Proportional Integral Controller
PWM	Pulse Width Modulation
SDC	Student Design Center
SVM	Space Vector Modulation
VARIAC	Variable Autotransformer
V_{DC}	DC Link Voltage

THIS PAGE INTENTIONALLY LEFT BLANK

EXECUTIVE SUMMARY

In this thesis, we emulate a Wind Turbine Generator by driving a Doubly Fed Induction Generator (DFIG) via a DC motor with variable input torque capability. Previous research has shown we can use a DFIG with back-to-back SVMs to accomplish a decoupled Supply-side, and DFIG-side, control scheme while allowing power flow to occur between the two systems.

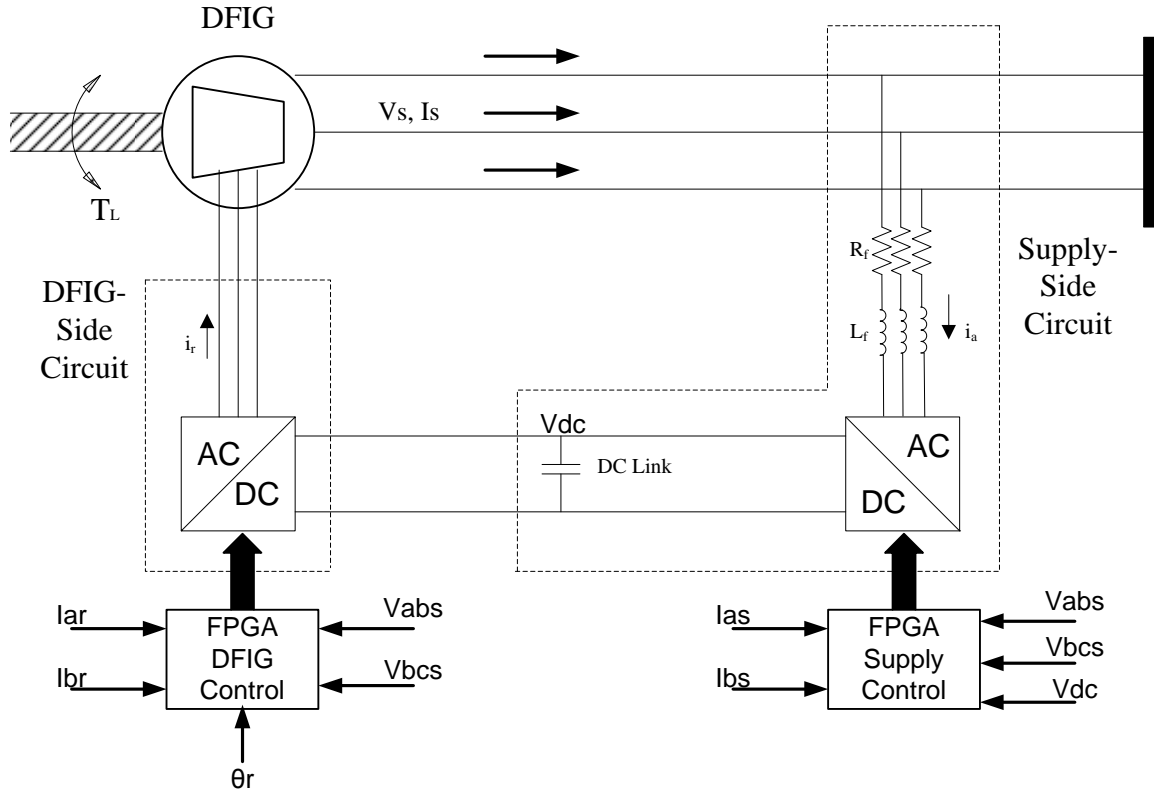
The two circuits of concern are the DFIG and Supply-side circuits. The DFIG and Supply-side circuits are electrically coupled with back-to-back (DFIG-side and Supply-side) Space Vector Modulators (SVMs) that are coupled through a DC Link consisting of a capacitor bank. The back-to-back SVMs, with DC Link, provide bi-directional power flow between the DFIG rotor and Supply-side power supply. Bi-directional power flow is achieved when the DFIG is controlled at supersynchronous speeds, and input torque is enough to overcome losses, and subsynchronous speeds (Supply-side provides power to the rotor).

The Supply-side power supply (3-phase AC) provides power to the Supply-side circuit (stepped down by a VARIAC) and the Stator of the DFIG. The Supply-side circuit senses the supply side voltage, current and DC Link voltage (VDC) and sends the sensed inputs to a Field Programmable Gate Array (FPGA). The FPGA is programmed via a Simulation software package called Simulink to achieve the desired control of the specified parameters. For the Supply-side circuit we use the mentioned sensed inputs to derive control of VDC so that it is maintained at 200V via SVM. There is also a built-in protection feature in the Supply-side circuit that will turn off the SVM if a VDC of 240V is reached.

The DFIG circuit power supply is provided by the DC Link and DFIG-side SVM. The DFIG circuit senses rotor current, stator voltage, rotor speed, and rotor electrical position (as provided by an encoder). These inputs, like the Supply-side circuit, are then sent to an FPGA which is programmed to control the DFIG parameters. The DFIG circuit will take the rotor speed input and derive a current reference that is used to control the

rotor speed using a Proportional Integral Controller (PI). It is important to show that we can control the DFIG rotor speed since traditional Wind Turbine Generators would use turbine blade pitch control in tandem with a synchronous generator to provide a constant speed, and hence a constant output frequency. Further, it is noteworthy that a wind-speed profile can be adapted to a specific Wind Turbine (outfitted with a DFIG) in order to program the DFIG to run at specified speeds for a given wind speed. This tool can be used to provide an optimized rotor speed for a given wind speed. For our application we will show that the DFIG rotor speed can be controlled (subsynchronous, synchronous or supersynchronous) for any given input torque and thus distributes the power generated by the DFIG as predicted between the rotor and stator. Further, this experiment will demonstrate the bi-directional power flow of the back-to-back SVMs showing power recovery via the DFIG rotor.

As illustrated in the below figure, the Supply-side SVM converts a 3-phase AC source to a constant DC Link voltage of 200V. The DC Link voltage is then inverted into a 3-phase waveform via the DFIG-Side SVM (during modes for which power is being delivered to the DFIG). The digital control for the Insulated Gate Bipolar Transistor (IGBT) network is implemented via the FPGA. The FPGA interface samples the rotor current and the stator voltage of the DFIG through an analog to digital (A/D) converter. There is an input from the encoder, θ_r , to provide the position and speed of the rotor to the FPGA through the interface circuit board. An algorithm then calculates the slip frequency of the DFIG which is used to derive the needed rotor current frequency and amplitude to maintain a specified rotor speed, and therefore a controllable output frequency.

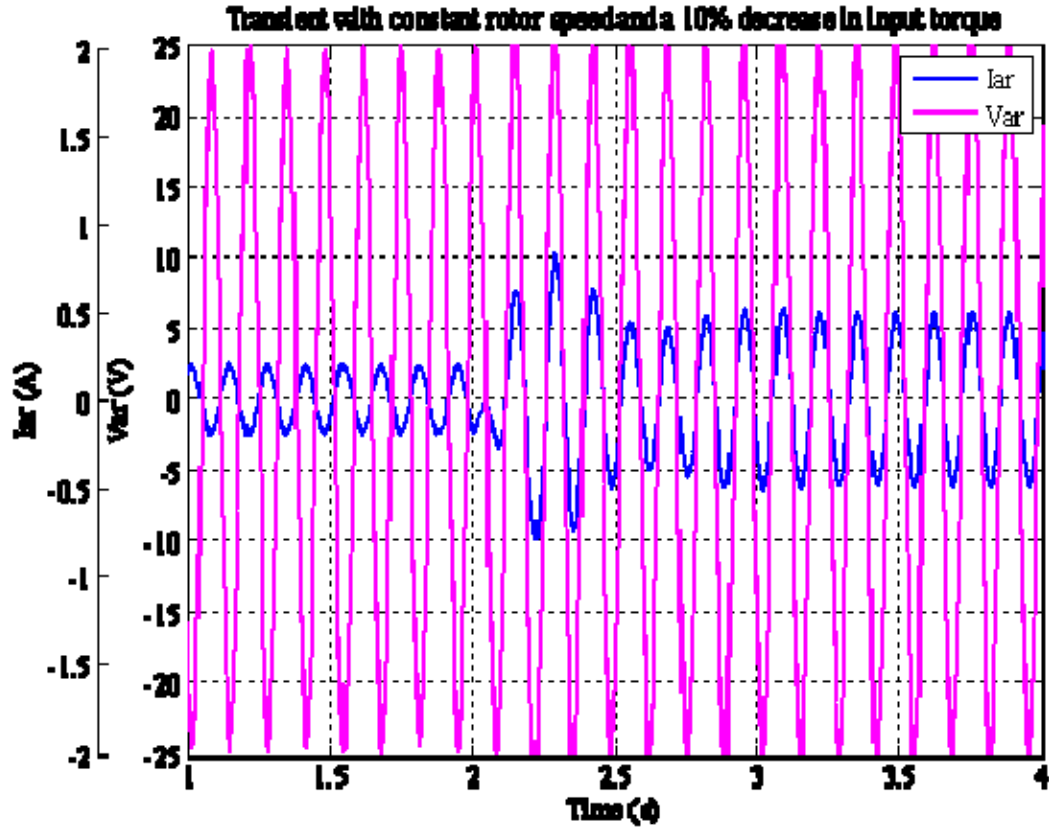


Simplified Circuit of Wind Turbine DFIG System.

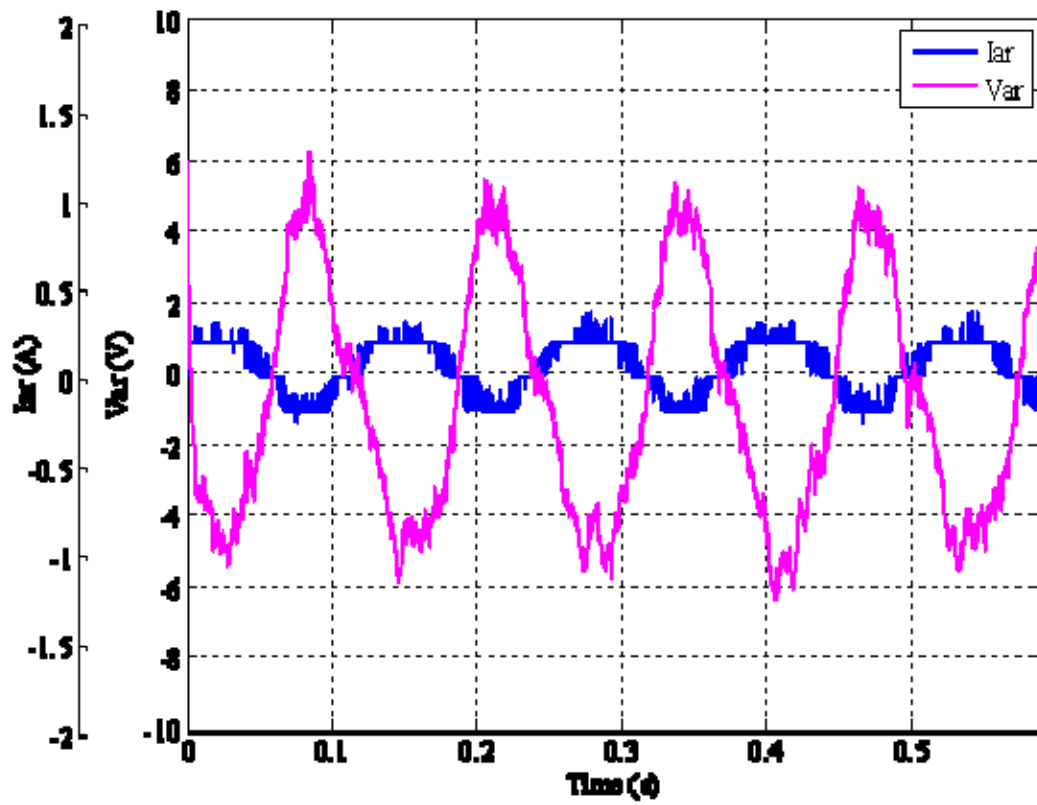
The below figure demonstrates an input torque transient representing a large wind gust. By commanding a specified supersynchronous speed, while taking into account windage and friction losses of the system, it is clear that the input torque transient produces a power flow reversal in the rotor. In other words, the rotor mode transitions from power flow from the rotor (negative rotor current) to power flow to the rotor (positive rotor current).

In addition, this transient plot (simulation model) shows a smooth transition as the power flow reverses between power flow from the rotor to power flow to the rotor. This transition is modeled using a constant commanded rotor speed along with a 10% decrease in input torque. The next two figures (experimental results) parallels this transition with the steady state captures corresponding to the simulation transient. The experimental results were run through a low pass filter with a corner frequency of 80 Hz in order to create a useful plot of the event. Due to windage and friction losses, a commanded

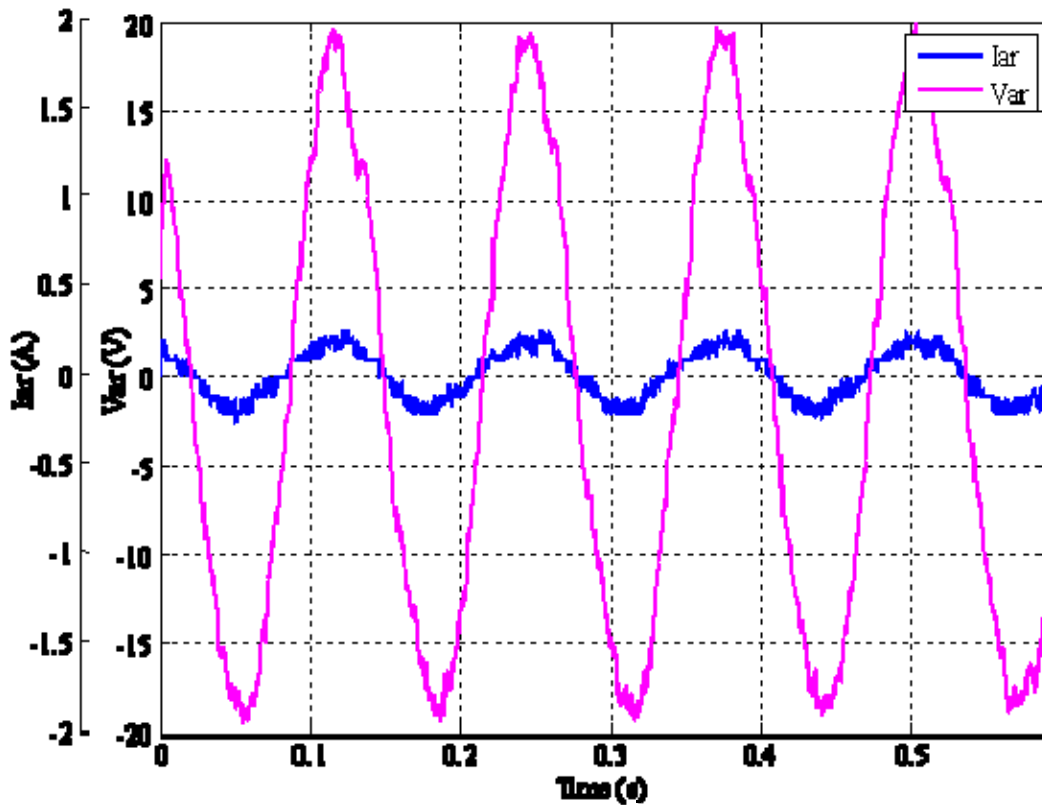
supersynchronous speed was ordered to achieve the power flow transition results during the constant rotor speed experiment. If the experimental results are closely examined, it is interesting to note the small, low frequency ripple due to speed control beating.



Simulation: Input Torque Transient Showing Rotor Power Reversal.



Experimental: Rotor Current and Voltage with Power Flow from the Rotor.



Experimental: Rotor Current and Voltage with Power Flow to the Rotor.

In conclusion, we showed that we can control the DFIG rotor excitation to provide a constant output frequency. Our application demonstrated that the DFIG rotor speed can be controlled (subsynchronous, synchronous or supersynchronous) for a given input torque and thus distributes the power generated by the DFIG as predicted between the rotor and stator. Finally, this experiment also demonstrates the bi-directional power flow of the back-to-back SVMs showing power recovery via the DFIG rotor.

ACKNOWLEDGEMENTS

I would like to thank the entire faculty and staff at the Naval Postgraduate School for providing me with outstanding support while attaining a higher education. Thank you to Professor Alexander Julian for your continual support, advice, and expansive knowledge that you passed on to me through my arduous endeavor to get the machinery running. Thank you to Warren Rogers for assisting me in a timely matter in the lab with the special tools needed to complete my research.

THIS PAGE INTENTIONALLY LEFT BLANK

I. INTRODUCTION

A. MISSION

In this thesis, we emulate a Wind Turbine Generator by driving a Doubly Fed Induction Generator (DFIG) via a DC motor with variable input torque capability. As discussed in [1-4] we can use a DFIG with back-to-back SVMs to accomplish a decoupled Supply-side, and DFIG-side, control scheme while allowing power flow to occur between the two systems. The control schemes developed with this research can branch into shipboard application as discussed below.

The benefits of researching and developing a Wind Turbine Generation System, refitted with a DFIG, span a wide range of purposes for the United States as a whole, as well as the United States military. In particular, there are several naval warships still running large, separately supplied, gas turbine generators to provide the ship with electrical power to vital loads. Considering this one example, a properly researched and developed DFIG with precision characteristic control can not only save space (in a space-scarce environment), but also provide a more efficient means of power distribution when mechanically coupled to the main propulsion gas turbine shaft line. This, of course, requires a variable speed constant frequency control scheme since the propulsion turbine shaft speed is variable according to the desired ship speed [5]. The applications of the DFIG are many and complex, but the simple example above shows a common sense approach to save space and fuel consumption for our United States military.

B. OBJECTIVE

The goal of this thesis was to build a computer simulation of a Wind Turbine Generation System, based on mathematical equations, through the use of Mathworks' Simulink software. Once the simulation was complete, the goal shifted to build a fully functioning model of a Wind Turbine Generation System. A series of experiments were performed to compare actual results with expected/simulation results. Once the series of experiments proved the simulation was an accurate depiction of the model, the machinery

was put to full test as a Wind Turbine Generation System to be used in future lab work and research to hone in features that could be discovered.

C. APPROACH

The first step is to generate a computer simulation of the system, shown in Figure 1. There are a number of ways to simulate the DFIG coupled with a Supply-side, via back-to-back SVMs, but the one used for this thesis is covered in [1]. Specifically, a computer model of the DFIG-side circuit based on mathematical equations is simulated in the rotor reference frame using dq0 transformation. The advantage of using dq0 transformation is most apparent when attempting to decouple DFIGs real and reactive power. By doing so, it is possible to separately control generator torque (hence speed) and reactive power (hence rotor and stator power factor) when the currents controlled are in the slip frequency reference frame. The DFIG-side circuit simulation inputs are input torque, stator voltage, rotor current, and rotor speed and position.

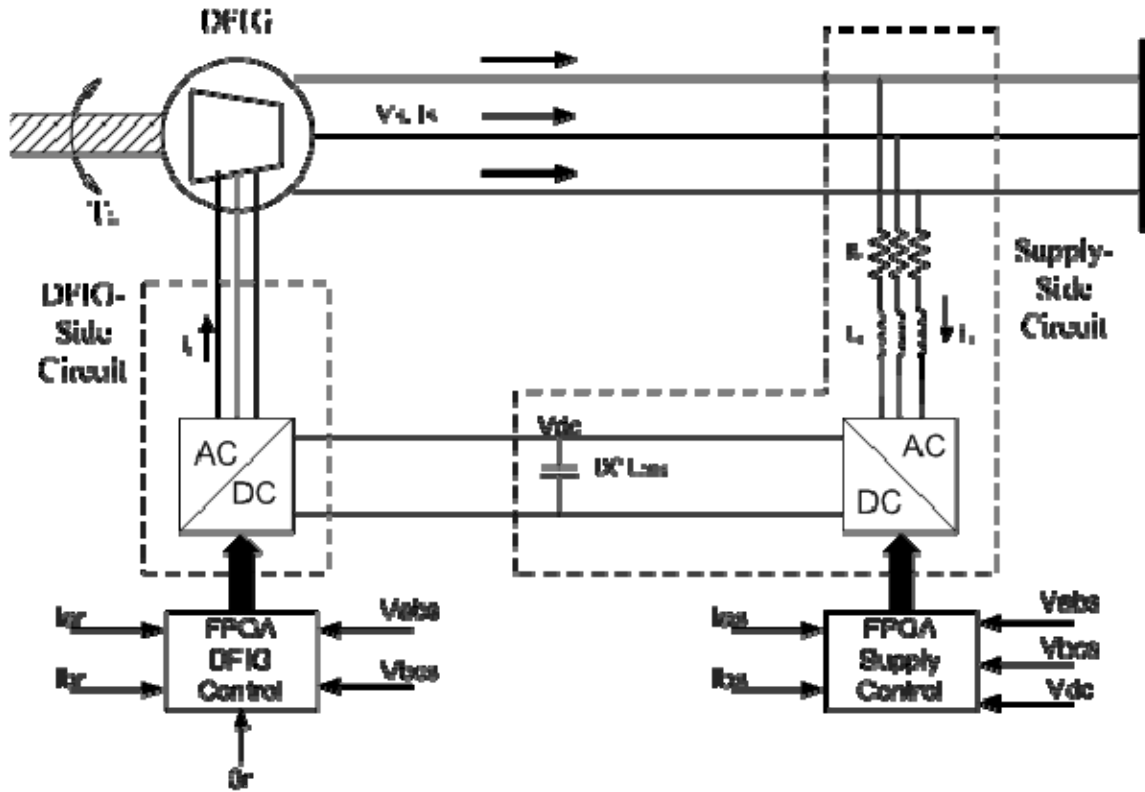


Figure 1. Simplified Circuit of Wind Turbine DFIG System.

The Supply-side circuit simulation is based in the stator reference frame using dq0 transformation. Not unlike the DFIG-side circuit, there is a distinct advantage in using the dq0 transformation so as to decouple real and reactive power on the Supply-side circuit. This, in turn, allows a separate control of DC Link voltage (via a current reference) and reactive power (hence Supply-side power factor). The Supply-side circuit simulation inputs are Supply-side voltage, DC Link voltage and Supply-side current.

The physical system consists of a DFIG, back-to-back SVMs, Student Design Center (SDC) [6], an encoder, and a DC motor used to simulate changes in wind speed. The DFIG is connected to the grid via the stator windings and to the DFIG-side SVM via the rotor windings. The SDC is the mechanism by which the control algorithm is implemented. The SDC measures the applicable system parameters and outputs the

appropriate control signals to the SVM to control the rotor currents in a fashion that allows for a specific mode of operation. For our application we will show that the DFIG rotor speed can be controlled (subsynchronous, synchronous or supersynchronous) for a given input torque and thus distributes the power generated by the DFIG as predicted between the rotor and stator.

D. THESIS ORGANIZATION

This thesis is organized with Chapter II covering the theory of induction machines; to include the equations that represent voltage, flux linkage, and reference frame transformations and how the voltage and flux equations and machine parameters are used to model the system. Chapter III is dedicated to the control algorithm. It explains how an algorithm is formulated, based on the equations derived in Chapter II, and is manipulated to control the simulation and the physical system. Chapter IV displays the results of the working system, and compares the actual results to the simulation results. Chapter IV also includes the testing procedure used to calibrate and implement the encoder and its offset, the method used to transform the DFIG-side rotor currents to a slip frequency reference frame, and Xilinx implementation methods. Chapter V discusses the conclusions and future research objectives for this thesis. The Appendix contains Matlab files, data sheets for equipment used, specific schematic layout of the Simulink systems, and transformation derivations used in this thesis.

II. DFIG THEORY

A. INDUCTION MACHINE EQUATIONS

Simulink is a powerful tool that can be implemented in the simulation of any given system that can be mathematically represented. To understand the simulation of the Wind Turbine Generation System, refitted with a DFIG, there must be a thorough understanding of the equations that represent the DFIG. The equations used to characterize the DFIG are obtained from [7]. The induction machine voltage equations are expressed as

$$\begin{aligned} [v_{abc_s}] &= [r_s][i_{abc_s}] + \rho[\lambda_{abc_s}] \\ [v_{abc_r}] &= [r_r][i_{abc_r}] + \rho[\lambda_{abc_r}] \end{aligned} \quad (1)$$

where the subscript s and r are denoting the stator and rotor associated variables and λ represents the flux linkage. Finally, ρ is used as the derivative operator. For a magnetically linear system, flux linkage can be represented as equation (2).

$$\begin{bmatrix} \lambda_{abc_s} \\ \lambda_{abc_r} \end{bmatrix} = \begin{bmatrix} L_s & L_{sr} \\ (L_{sr})^T & L_r \end{bmatrix} \begin{bmatrix} i_{abc_s} \\ i_{abc_r} \end{bmatrix} \quad (2)$$

where L_{sr} represents the mutual inductance between the stator and rotor. The stator, rotor and mutual winding inductances are

$$L_s = \begin{bmatrix} L_{ls} + L_{ms} & -\frac{1}{2}L_{ms} & -\frac{1}{2}L_{ms} \\ -\frac{1}{2}L_{ms} & L_{ls} + L_{ms} & -\frac{1}{2}L_{ms} \\ -\frac{1}{2}L_{ms} & -\frac{1}{2}L_{ms} & L_{ls} + L_{ms} \end{bmatrix} \quad (3)$$

$$L_r = \begin{bmatrix} L_{lr} + L_{mr} & -\frac{1}{2}L_{mr} & -\frac{1}{2}L_{mr} \\ -\frac{1}{2}L_{mr} & L_{lr} + L_{mr} & -\frac{1}{2}L_{mr} \\ -\frac{1}{2}L_{mr} & -\frac{1}{2}L_{mr} & L_{lr} + L_{mr} \end{bmatrix} \quad (4)$$

$$L_{sr} = L_{sr} \begin{bmatrix} \cos \theta_r & \cos(\theta_r + \frac{2\pi}{3}) & \cos(\theta_r - \frac{2\pi}{3}) \\ \cos(\theta_r - \frac{2\pi}{3}) & \cos \theta_r & \cos(\theta_r + \frac{2\pi}{3}) \\ \cos(\theta_r + \frac{2\pi}{3}) & \cos(\theta_r - \frac{2\pi}{3}) & \cos \theta_r \end{bmatrix} \quad (5)$$

where the variables L_{ls} and L_{ms} are the leakage and magnetizing inductances of the stator windings; conversely, L_{lr} and L_{mr} are the leakage and magnetizing inductances for the rotor windings. Lastly, θ_r is the angular position of the rotor.

When creating an equivalent circuit, a standard convention is to refer the rotor variables to the stator windings using the appropriate turn ratio N .

$$i'_{abc} = \frac{N_r}{N_s} i_{abc} \quad (6)$$

$$v'_{abc} = \frac{N_s}{N_r} v_{abc} \quad (7)$$

$$\lambda'_{abc} = \frac{N_s}{N_r} \lambda_{abc} \quad (8)$$

$$r' = \left(\frac{N_s}{N_r} \right)^2 r_r \quad (9)$$

This turns ratio referral also applies to the magnetizing and mutual inductances and are related by

$$L_{ms} = \frac{N_s}{N_r} L_{sr} \quad (10)$$

$$L'_r = \left(\frac{N_s}{N_r} \right)^2 L_r \quad (11)$$

$$L'_{lr} = \left(\frac{N_s}{N_r} \right)^2 L_{lr} \quad (12)$$

where by defining $L'_{sr} = \frac{N_s}{N_r} L_{sr}$ and $L'_{mr} = \left(\frac{N_s}{N_r} \right)^2 L_{mr}$ the rotor inductance variables can be referred to the stator windings as shown in equations (13) and (14).

$$L'_{sr} = L_{ms} \begin{bmatrix} \cos \theta_r & \cos(\theta_r + \frac{2\pi}{3}) & \cos(\theta_r - \frac{2\pi}{3}) \\ \cos(\theta_r - \frac{2\pi}{3}) & \cos \theta_r & \cos(\theta_r + \frac{2\pi}{3}) \\ \cos(\theta_r + \frac{2\pi}{3}) & \cos(\theta_r - \frac{2\pi}{3}) & \cos \theta_r \end{bmatrix} \quad (13)$$

$$L'_r = \begin{bmatrix} L'_{lr} + L_{ms} & -\frac{1}{2}L_{ms} & -\frac{1}{2}L_{ms} \\ -\frac{1}{2}L_{ms} & L'_{lr} + L_s & -\frac{1}{2}L_{ms} \\ -\frac{1}{2}L_{ms} & -\frac{1}{2}L_{ms} & L'_{lr} + L_{ms} \end{bmatrix} \quad (14)$$

The flux linkage and voltage equations in (1) and (2), in terms of variables referred to the stator windings, can now be expressed as

$$\begin{bmatrix} \lambda_{abcs} \\ \lambda'_{abcr} \end{bmatrix} = \begin{bmatrix} L_s & L'_{sr} \\ (L'_{sr})^T & L'_r \end{bmatrix} \begin{bmatrix} i_{abcs} \\ i'_{abcr} \end{bmatrix} \quad (15)$$

$$\begin{aligned} [v_{abcs}] &= [r_s][i_{abcs}] + \rho[\lambda_{abcs}] \\ [v'_{abcr}] &= [r'_r][i'_{abcr}] + \rho[\lambda'_{abcr}] \end{aligned} \quad (16)$$

Above, the physical voltage equations were given for the induction machine; however, in an effort to reduce the complexity of their differential equations we will use a change of variables transformation to a new reference frame as described in equation (17).

$$\begin{aligned} [f_{qd0s}^x] &= K_s^x [f_{abcs}] \\ [f'_{qd0r}^x] &= K_r^x [f'_{abcr}] \end{aligned} \quad (17)$$

where the matrix K_s for stator variables and K_r for rotor variables is expressed as

$$K_s = \frac{2}{3} \begin{bmatrix} \cos \theta & \cos\left(\theta - \frac{2\pi}{3}\right) & \cos\left(\theta + \frac{2\pi}{3}\right) \\ \sin \theta & \sin\left(\theta - \frac{2\pi}{3}\right) & \sin\left(\theta + \frac{2\pi}{3}\right) \\ \frac{1}{2} & \frac{1}{2} & \frac{1}{2} \end{bmatrix} \quad (18)$$

$$K_r = \frac{2}{3} \begin{bmatrix} \cos \beta & \cos\left(\beta - \frac{2\pi}{3}\right) & \cos\left(\beta + \frac{2\pi}{3}\right) \\ \sin \beta & \sin\left(\beta - \frac{2\pi}{3}\right) & \sin\left(\beta + \frac{2\pi}{3}\right) \\ \frac{1}{2} & \frac{1}{2} & \frac{1}{2} \end{bmatrix}$$

$$\beta = \theta - \theta_r \quad (19)$$

In equations (18) and (19), θ is the variable used to transform the f_{abc} variables for which equation (17) are referred. The place holder x in equation (17) represents this particular frame of reference that variables are transformed. The place holder f represents the voltage, current, or flux linkages in the stator or rotor windings. If no place holder is used then the reference frame is considered to be an arbitrary frame of reference. When transforming between reference frames equation (20) is utilized where y represents the new frame of reference.

$${}^x K^y = \begin{bmatrix} \cos(\theta_y - \theta_x) & \sin(\theta_y - \theta_x) & 0 \\ -\sin(\theta_y - \theta_x) & \cos(\theta_y - \theta_x) & 0 \\ 0 & 0 & 1 \end{bmatrix} \quad (20)$$

After performing the transformation of equation (17) on each component in the matrices on the right hand side of equation (16), the voltage equations can now be expressed in the arbitrary reference frame as

$$\begin{aligned}
v_{qs} &= r_s i_{qs} + \omega \lambda_{ds} + \rho \lambda_{qs} \\
v_{ds} &= r_s i_{ds} - \omega \lambda_{qs} + \rho \lambda_{ds} \\
v_{0s} &= r_s i_{0s} + \rho \lambda'_{0r} \\
v'_{qr} &= r'_r i'_{qr} + (\omega - \omega_r) \lambda'_{qr} + \rho \lambda'_{qr} \\
v'_{dr} &= r'_r i'_{dr} - (\omega - \omega_r) \lambda'_{dr} + \rho \lambda'_{dr} \\
v'_{0r} &= r'_r i'_{0r} + \rho \lambda'_{0r}
\end{aligned} \tag{21}$$

In equation (21), ω_r is electrical angular frequency of the rotor, and ω is the angular frequency of the reference frame that the variables are transformed in radians per second. Since $\psi = \lambda \omega_b$ and $\omega_b = 2\pi 60 \text{ rad/sec}$, it is convenient to express the inductance component of the flux linkages in equation (21) as a reactance instead of as an inductance, beginning with equation (22).

$$\begin{aligned}
v_{qs} &= r_s i_{qs} + \frac{\omega}{\omega_b} \psi_{ds} + \frac{\rho}{\omega_b} \psi_{qs} \\
v_{ds} &= r_s i_{ds} - \frac{\omega}{\omega_b} \psi_{qs} + \frac{\rho}{\omega_b} \psi_{ds} \\
v_{0s} &= r_s i_{0s} + \frac{\rho}{\omega_b} \psi_{0s} \\
v'_{qr} &= r'_r i'_{qr} + \frac{(\omega - \omega_r)}{\omega_b} \psi'_{dr} + \frac{\rho}{\omega_b} \psi'_{qr} \\
v'_{dr} &= r'_r i'_{dr} - \frac{(\omega - \omega_r)}{\omega_b} \psi'_{qr} + \frac{\rho}{\omega_b} \psi'_{dr} \\
v'_{0r} &= r'_r i'_{0r} + \frac{\rho}{\omega_b} \psi'_{0r}
\end{aligned} \tag{22}$$

The flux linkage component of equation (21) now has units of flux linkage per second and represented by the symbol ψ . For ease of understanding the flux linkages in (21) and flux linkage per second in (22) are compared in equations (23) and (24).

$$\begin{aligned}
\lambda_{qs} &= L_{ls} i_{qs} + L_{ms} (i_{qs} + i'_{qr}) \\
\lambda_{ds} &= L_{ls} i_{ds} + L_{ms} (i_{ds} + i'_{dr}) \\
\lambda_{0s} &= L_{ls} i_{0s} \\
\lambda'_{qr} &= L_{lr} i_{qr} + L_{ms} (i_{qs} + i'_{qr}) \\
\lambda'_{dr} &= L_{lr} i_{dr} + L_{ms} (i_{ds} + i'_{dr}) \\
\lambda'_{0r} &= L_{lr} i'_{0r}
\end{aligned} \tag{23}$$

$$\begin{aligned}
\psi_{qs} &= X_{ls} i_{qs} + X_{ms} (i_{qs} + i'_{qr}) \\
\psi_{ds} &= X_{ls} i_{ds} + X_{ms} (i_{ds} + i'_{dr}) \\
\psi_{0s} &= X_{ls} i_{0s} \\
\psi'_{qr} &= X'_{lr} i_{qr} + X_{ms} (i_{qs} + i'_{qr}) \\
\psi'_{dr} &= X'_{lr} i_{dr} + X_{ms} (i_{ds} + i'_{dr}) \\
\psi'_{0r} &= X'_{lr} i'_{0r}
\end{aligned} \tag{24}$$

The above equations mathematically represent the behavior of a DFIG, and are used in the simulation process to arrive at an appropriate physical model that will be discussed below. More can be read concerning induction machine theory as used in this thesis application in [4].

B. SYSTEM CONFIGURATION

The combined system is shown in Figure 1. The DFIG is a 175W, 120V, 60Hz, 4-pole machine with parameters listed in the Appendix data sheet. The system parameters were used in order to effectively model the system in Simulink. The Lab-Volt model 8231 was used as the DFIG. The stator consists of 3-phase wye-connected windings with a turns ratio of $N_s/N_r = 10$ and resistance $R_s = 12\Omega$. The rotor consists of 3-phase wye-connected windings with resistance $R_r = 4\Omega$. The reactance of the DFIG are $X_m = 180\Omega$ and $X_{ls} = X_{lr} = 9\Omega$.

The DC motor used to emulate the wind turbine is the Lab-Volt 8211. It is a 175W, 120V, 4-pole machine with a nominal operating speed of 1800 RPM. The operating speed range used was 1350 RPM to 2150 RPM.

The power supply used for the experiments was the Lab-Volt 8821-10. It is a 3-phase 120V to 208V AC power supply with a separate VARIAC power supply and 120V DC power supply. In order to properly provide power to the Supply-side circuit, the VARIAC output is used for the Supply-side SVM with a nominal setting of 60V rms. This allows sufficient voltage to be boosted to maintain the DC Link at 200V without excessive current transients. Further, a set of 640 μ H inductors were placed in series (see Figure 2.) to the input of the SVM in order to decouple the current sensors in the SDC from the switching action of the SVM.

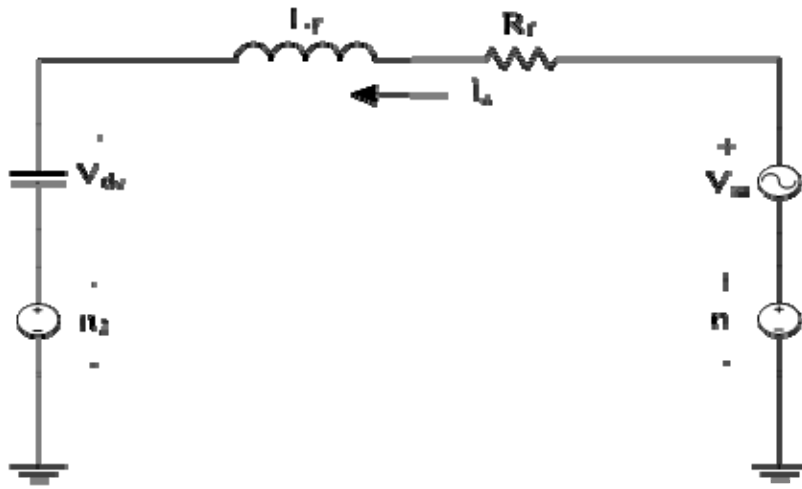


Figure 2. Simplified Single Phase Circuit Showing the Inductor Connections.

The mathematical analysis used to arrive at the equivalent simulation matrices used in Simulink are shown in equations (25)–(31). The single phase neutral point voltages are

$$V_{an2} + V_{bn2} + V_{cn2} = 3n_1 - 3n_2 = 3_{CM} \text{ volts} \quad (25)$$

and the KVL analysis results in

$$V_{an2} + sL_f i_a + R_f i_a = V_{san1} + (n_1 - n_2) \quad (26)$$

$$V_{bn2} + sL_f i_b + R_f i_b = V_{sbn1} + (n_1 - n_2) \quad (27)$$

$$V_{cn2} + sL_f i_c + R_f i_c = V_{scn1} + (n_1 - n_2) \quad (28)$$

Where n_1 and n_2 are neutral point voltages.

Subtracting (26) and (27) gives

$$V_{an2} - V_{bn2} + sL_f (i_a - i_b) + R_f (i_a - i_b) = V_{san1} - V_{sbn1} \quad (29)$$

and subtracting (27) and (28) gives

$$V_{bn2} - V_{cn2} + sL_f (i_b - i_c) + R_f (i_b - i_c) = V_{sbn1} - V_{scn1} \quad (30)$$

Defining $V_{an2} - V_{bn2} = V_{dc_ab}$, $V_{bn2} - V_{cn2} = V_{dc_bc}$, and $i_a + i_b + i_c = 0$ the matrix yields

$$\begin{bmatrix} V_{dc_ab} \\ V_{dc_bc} \end{bmatrix} + sL_f \begin{bmatrix} 1 & -1 \\ 1 & 2 \end{bmatrix} \begin{bmatrix} i_a \\ i_b \end{bmatrix} + R_f \begin{bmatrix} 1 & -1 \\ 1 & 2 \end{bmatrix} \begin{bmatrix} i_a \\ i_b \end{bmatrix} = \begin{bmatrix} V_{sab} \\ V_{sbc} \end{bmatrix} \quad (31)$$

Next, equation (31) can be put into a state space form by defining

$$N = L_f \begin{bmatrix} 1 & -1 \\ 1 & 2 \end{bmatrix} \quad M = R_f \begin{bmatrix} 1 & -1 \\ 1 & 2 \end{bmatrix} \quad P = \begin{bmatrix} 1 \\ 1 \end{bmatrix} \quad \begin{bmatrix} V_{dc_ab} - V_{sab} \\ V_{dc_bc} - V_{sbc} \end{bmatrix} = \begin{bmatrix} V_{ab} \\ V_{bc} \end{bmatrix}$$

So that (31) can be written as

$$Mx + sNx + Pu = 0. \quad (32)$$

Then the state space model becomes

$$sx = Ax + Bu \quad (33)$$

with

$$\begin{aligned} A &= -N^{-1}M \\ B &= -N^{-1}P \end{aligned} \quad (34)$$

Therefore, the matrices used in Simulink are

$$s \begin{bmatrix} i_a \\ i_b \end{bmatrix} = - \begin{bmatrix} L_f & -L_f \\ L_f & 2L_f \end{bmatrix}^{-1} \begin{bmatrix} R_f & -R_f \\ R_f & 2R_f \end{bmatrix} \begin{bmatrix} i_a \\ i_b \end{bmatrix} - \begin{bmatrix} L_f & -L_f \\ L_f & 2L_f \end{bmatrix}^{-1} \begin{bmatrix} 1 \\ 1 \end{bmatrix} \begin{bmatrix} V_{ab} \\ V_{bc} \end{bmatrix} \quad (35)$$

The above process represents the common approach used to parallel circuit analysis and Simulink modeling. Since Simulink is a mathematical based simulation program, vice any given circuit solving based program, it is imperative to accurately analyze the mathematical characteristics of any given subsystem in order to effectively implement Simulink.

Once an in depth understanding of induction machine theory and system configuration was established, specific control methods were explored. The control methods included control components, Supply-side control, DFIG-side control, SVM scheme concepts, and the encoder implementation.

THIS PAGE INTENTIONALLY LEFT BLANK

III. CONTROLLER SCHEME

A. CONTROLLER COMPONENTS

The back-to-back SVM components used for this research are a combined package manufactured by SEMIKRON. The package is called the SEMISTACK-IGBT and consists of a three phase inverter that is coupled to the DC Link capacitor bank. The inverters inside the SEMISTACK are made of SKM 50 GB 123D IGBTs that are controlled by SEMIKRON SKHI 22 gate drivers. The Supply-side SEMISTACK is used to maintain the DC Link at 200V and can also be used to control the power factor to the grid when in inverter mode. Controlling the grid power factor was not within the scope of this thesis, outside of experimentally showing its explicit control, but is a feature that can be used to minimize transmission losses in a large scale project. The control for each IGBT in the SEMISTACK is implemented through the SDC. Two SDCs are utilized (Supply-side and DFIG-side) and include a Xilinx FPGA and a Control board that has various inputs and outputs that interface with the Supply-side and DFIG-side circuits. One of the inputs is an 8-channel, 12-bit A/D converter used to measure the voltage and current signals from their associated systems. The DFIG-side circuit also has a 4-pin input that samples the rotor encoder pulse waveforms and converts them into a rotor position and rotor speed input via an algorithm implemented in SIMULINK. The FPGA is programmed to take the sampled inputs and generate the desired gate signals to the control board. The control board has BNC (Bayonette Neil-Concealman) connectors that connect to the SEMISTACK's gate drivers. The gate drive signals activate the IGBTs in a fashion that will produce the desired 3-phase current in the rotor windings for the DFIG-side, or the commanded DC Link voltage for the Supply-side. The procedure for using the SDC, architecture of internal components, and the benefits of using FPGA for digital control of power systems is discussed in [6].

B. SUPPLY-SIDE CONTROLLER

The Supply-side circuit is powered via a 3-phase AC power supply stepped down by a VARIAC to 60V rms. Of note, it is important to calculate the DC Link injection

voltage as described in [2]. The injected voltage should be less than $V_{DC_max} / 2\sqrt{2}$, which corresponds to an injected voltage of 60V rms. There is a set of three inductors connected in series to the SEMISTACK, downstream of the Supply-side SDC, which decouples the SDC sensors from the switching action of the IGBTs. Figure 1. shows, and equations (25) through (35) describe their matrix analysis. The SDC senses the stepped down power supply line-to-line voltages, V_{AB} and V_{BC} , and derives the Supply-side voltage angle, θ_s , as shown in Figure 3.

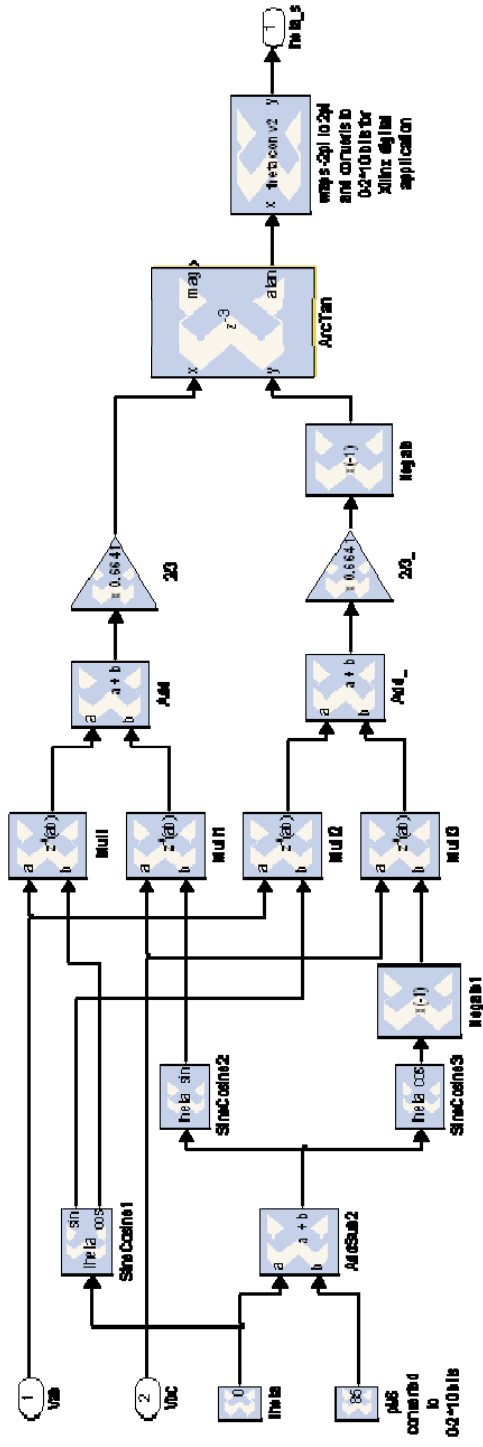


Figure 3. Simulink Model of Supply-side Voltage Angle Calculation.

Since the SDC only has four voltage inputs it is important to be efficient about the voltage input configuration. Further, it is not always convenient to input single phase values due to the difficulty, at times, to tap a neutral point. This is why it is suitable to use the line-to-line voltage parameters as inputs. The derivation of the V_{AB} and V_{BC} based voltage angle calculation as described in [7] and [8] is

$$v_{ab} = v_a - v_b; v_{bc} = v_b - v_c = v_b - (-v_a - v_b); \quad (36)$$

Note also that $i_a + i_b + i_c = 0$ for a wye connected winding set.

Placing into matrix form

$$\begin{bmatrix} v_{ab} \\ v_{bc} \end{bmatrix} = \begin{bmatrix} 1 & -1 \\ 1 & 2 \end{bmatrix} \begin{bmatrix} v_a \\ v_b \end{bmatrix} \Rightarrow \begin{bmatrix} v_a \\ v_b \end{bmatrix} = \frac{1}{3} \begin{bmatrix} 2 & 1 \\ -1 & 1 \end{bmatrix} \begin{bmatrix} v_{ab} \\ v_{bc} \end{bmatrix} \quad (37)$$

We define the matrix in dq0 terms using

$$\begin{aligned} v_q &= \frac{2}{3} \left[v_a \cos(\theta) + v_b \cos\left(\theta - \frac{2\pi}{3}\right) + v_c \cos\left(\theta + \frac{2\pi}{3}\right) \right] \\ &= \frac{2}{3} \left[v_a \cos(\theta) + v_b \cos\left(\theta - \frac{2\pi}{3}\right) + (-v_a - v_b) \cos\left(\theta + \frac{2\pi}{3}\right) \right] \\ &= \frac{2}{3} \left[v_a \left(\cos(\theta) - \cos\left(\theta + \frac{2\pi}{3}\right) \right) + v_b \left(\cos\left(\theta - \frac{2\pi}{3}\right) - \cos\left(\theta + \frac{2\pi}{3}\right) \right) \right] \end{aligned} \quad (38)$$

and

$$\begin{aligned} v_d &= \frac{2}{3} \left[v_a \sin(\theta) + v_b \sin\left(\theta - \frac{2\pi}{3}\right) + v_c \sin\left(\theta + \frac{2\pi}{3}\right) \right] \\ &= \frac{2}{3} \left[v_a \sin(\theta) + v_b \sin\left(\theta - \frac{2\pi}{3}\right) + (-v_a - v_b) \sin\left(\theta + \frac{2\pi}{3}\right) \right] \\ &= \frac{2}{3} \left[v_a \left(\sin(\theta) - \sin\left(\theta + \frac{2\pi}{3}\right) \right) + v_b \left(\sin\left(\theta - \frac{2\pi}{3}\right) - \sin\left(\theta + \frac{2\pi}{3}\right) \right) \right] \end{aligned} \quad (39)$$

After combining terms the line-to-line voltage equations become

$$\begin{bmatrix} v_q \\ v_d \end{bmatrix} = \frac{2}{3} \begin{bmatrix} \cos(\theta_e) & \sin(\theta_e + \pi/6) \\ \sin(\theta_e) & -\cos(\theta_e + \pi/6) \end{bmatrix} \begin{bmatrix} v_{ab} \\ v_{bc} \end{bmatrix} \quad (40)$$

Finally, θ_s is calculated using the ArcTan function with v_q and v_d as the inputs for the angle calculation. The ArcTan function gives an output from -2π to 2π . Since Xilinx is a digital bit-wise based program, it is necessary to implement the last block of Figure 3, which converts the ArcTan output to a wrapped 0 to 2^{10} bit output. The *thetaconv2* block code is listed in the Appendix.

The SDC sends the sensed power supply voltages and currents and processes the data in order to send the correct gate signal sequence to the SEMISTACK BNC connections. The IGBTs will gate on and off and send the supplied voltage to an internal capacitor bank, which supplies the DC Link terminals. Of note, each SEMISTACK has its own capacitor bank, and their associated external terminals, which is used to physically couple the Supply-side and DFIG-side DC link to form a common V_{DC} . The last Supply-side circuit input is V_{DC} , which is sent to the SDC as well. This, of course, is used to sense and maintain DC Link voltage at 200V. It is also used in a protection feature that shuts off the gate signals to the Supply-side SEMISTACK in the case that DC Link voltages reach 240V. The implementation of this protection feature utilizes an SR Flip-Flop.

In order to effectively control the DC Link voltage an inner and outer PI controller scheme is used. The outer loop controller senses V_{DC} , as compared to the V_{DC} reference of 200V, and generates a DC reference current (i_{q_ref}) that is sent to the inner loop. The inner loop is controlled in the qd0 synchronous reference frame so as to easily compare i_{q_ref} to the measured i_q in DC terms. The derived θ_s is now used as the β input, equation (19), for the qd0 equation to transform the supplied currents into the synchronous reference frame. Figure 4 shows the inner and outer loop Simulink model.

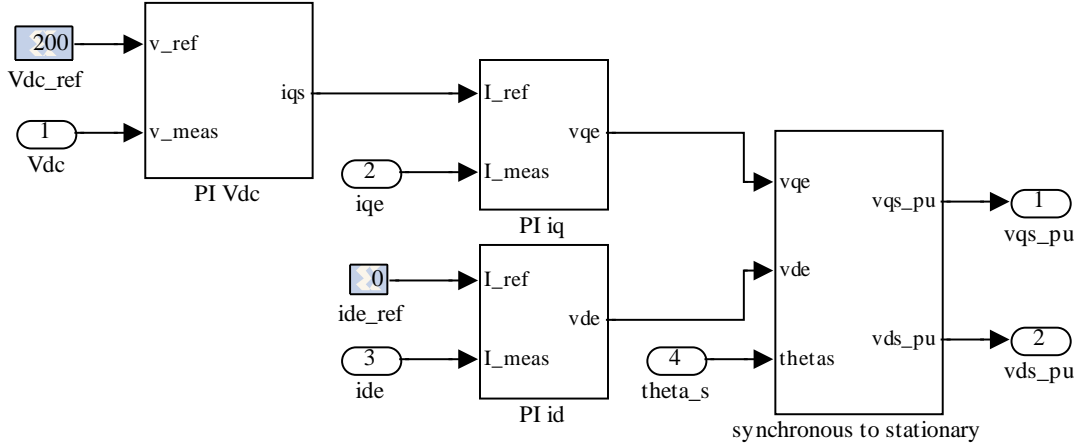


Figure 4. Inner and Outer PI Control Loops for the Supply-side Controller.

C. DFIG-SIDE CONTROLLER

The DFIG rotor is powered via the DFIG-side SEMISTACK IGBTs through the DC Link. The DFIG stator is powered via a 3-phase AC, 120V, 60Hz power supply corresponding with a grid. There is a set of three inductors connected in series to the SEMISTACK, downstream of the DFIG-side SDC, which decouples the SDC sensors from the switching action of the IGBTs. The SDC senses the stator line-to-line voltages, V_{AB} and V_{BC} , and transforms them into the $qd0$ rotor reference frame using θ_r (from the encoder) as β in equation (19). With the stator line-to-line voltages transformed to the $dq0$ rotor reference frame, the DFIG slip angle and frequency can be derived using the same method as described in the Supply-side controller section using the ArcTan function with v_q and v_d as the inputs for the angle calculation. The DFIG slip angle (θ_{slip}) is important since it will be used to control the DFIG in a synchronously rotating $dq0$ reference frame, with the q -axis oriented along the stator-flux vector position. This, in turn, enables decoupled control of the electrical torque (i_{qr}) and rotor excitation current (i_{dr}). Traditionally, θ_{slip} is obtained using the ArcTan function with a rotor referenced ψ_{qs} and ψ_{ds} as inputs, along with a $\pi/2$ offset, in place of the ArcTan calculation using v_q and v_d as the inputs for the angle calculation. The offset is associated with the relationship

between current and flux linkage as it relates to voltage. Since the θ_{slip} calculation used in this thesis is based on voltage, no offset is needed. The voltage based calculation of θ_{slip} requires a less complex algorithm, and thus less processing, than the flux linkage based θ_{slip} calculation. Both experimental and simulated tests were performed to compare the two θ_{slip} methods. In either test there was no detectable difference in the results for this model's application. Further tests should be performed to determine the extent of constraint between the two methods and either's benefits. Figure 5 shows an overview model of the slip angle calculation. The internals of this model can be sufficiently described by reviewing Figure 3.

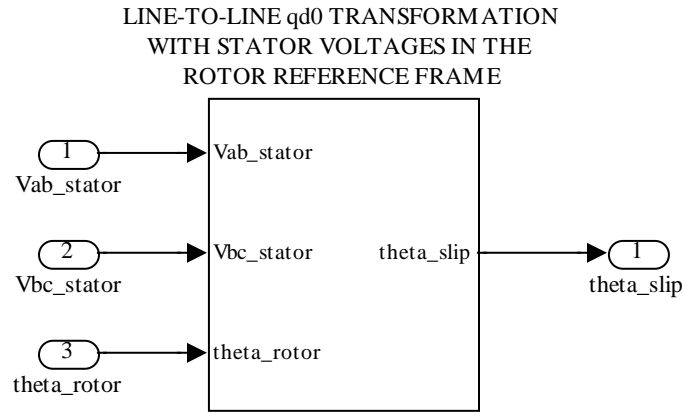


Figure 5. Simulink Model of DFIG-side Slip Angle Calculation.

In addition to the SDC sensing the stator line-to-line voltages, it also senses the phase A and B rotor currents (phase C is derived using phases A and B). The rotor currents are utilized, along with rotor angular frequency (w_r), to form the current control loops for the DFIG. The DFIG PI control loops consist of an outer loop and an inner loop. The outer loops takes w_r as an input and compares it to a commanded w_{r_ref} . The resulting difference passes through the speed PI controller and sends a reference current (i_{qr_ref}) to the current control loop, or inner loop. The reference current passes through the current PI controller and compares it to the measured i_{qr} . The resulting waveform is

converted to a per unit value and sent to the SVM block, which generates the gate signal sequence for the DFIG-side SEMISTACK. The current control loop is used to command a specified w_r as controlled via i_{qr} , or rotor excitation current via i_{dr} . Rotor angular position and speed are derived from the encoder, which will be discussed later. Figure 6 shows the DFIG controller topology.

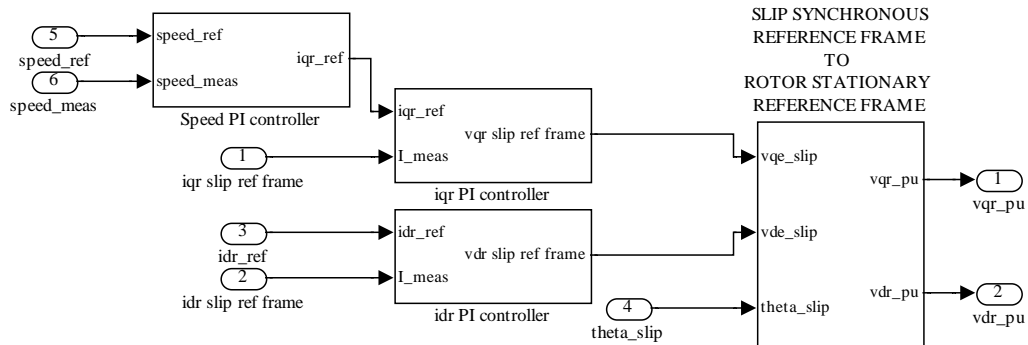


Figure 6. SIMULINK DFIG Controller Topology.

Both the Supply-side and DFIG-side controllers have unique differences up to their respective outputs, however, both controller outputs go to the exact same SVM architecture in order to control their commanded parameters.

D. SPACE VECTOR MODULATION

The modulation scheme used to create the desired 3-phase waveforms for the Supply-side and DFIG-side circuits is SVM. SVM is a specific form of Pulse Width Modulation (PWM) in which an algorithm involving space vectors are used to control the on and off times of pulsed signals. The generated signals then drive the IGBT gate signals to the SEMISTACK allowing the user to create a waveform of any magnitude and frequency desired. The SVM approach utilized in this controller is obtained from [8-9].

The SEMISTACK produces a 3-phase output voltage, as supplied from the DC Link, that is controlled by turning on and off its six IGBTs. Figure 7 shows both the

SEMISTACK-IGBT configuration and SVM Hexagon for which the on and off switching states are based on. The qd -axis is overlaid on the SVM Hexagon and represents the axis of the stationary reference frame variables v_{qr}^s and v_{dr}^s , which are shown entering the SVM block. The magnitude of the vectors v_{qr}^s and v_{dr}^s is equal to the vector V^* and θ is equal to the ArcTan of the two vectors.

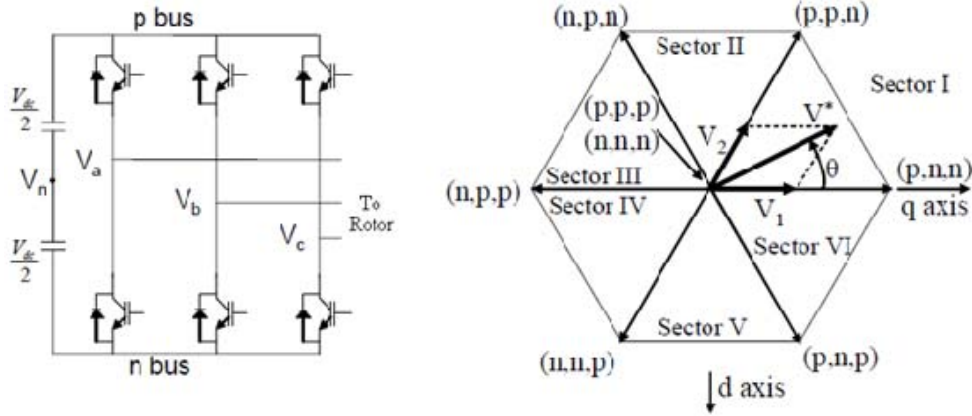


Figure 7. SEMISTACK-IGBTs and SVM Hexagon [From 8].

There are six sectors on the hexagon and eight possible on and off states that are used to produce the V^* vector. The vectors V_1 and V_2 , when summed, are also equal to the vector V^* . In Sector I, V_1 and V_2 correspond to the states (p, n, n) and (p, p, n) . The p and n correspond to the positive or negative IGBT bus signals for the respective phases V_a , V_b , and V_c . The zero vectors, which are represented by the states (p, p, p) and (n, n, n) , are not shown but are represented as vectors into and out of the page. The magnitude of the vectors V_1 and V_2 correspond to the amount of time spent on the switching states in each sector. The duty cycles T_1 and T_2 are the times spent on each cycle for the vectors V_1 and V_2 . The total time spent for one switching period is T_s

$$V_1 = \frac{2T_1V_{dc}}{3T_s} \quad (41)$$

$$V_2 = \frac{2T_2V_{dc}}{3T_s} \quad (42)$$

The law of sines on any one of the sectors in SVM Hexagon will produce

$$\frac{2V^*}{\sqrt{3}} = \frac{V_1}{\sin(60^\circ - \theta)} = \frac{V_2}{\sin(\theta)} \quad (43)$$

and substituting equations (41) and (42) into (43) is used to find the time of the duty cycles for the vectors V_1 and V_2

$$T_1 = \frac{V^* \sqrt{3}}{V_{dc}} T_s \sin(60^\circ - \theta) \quad (44)$$

$$T_2 = \frac{V^* \sqrt{3}}{V_{dc}} T_s \sin(\theta) \quad (45)$$

$$T_s = T_1 + T_2 + T_0 \quad (46)$$

SVM has the ability to minimize switching loss and harmonic distortion by controlling the order in which the states are applied so that only one gate is fired between sectors [8-9]. The switching pattern for each state and sector used in this thesis is shown in Table 1. The SVM algorithm is implemented inside each SDC where it is oversampled to converge on the performance of a true continuous sinusoidal signal. The digital implementation of the SVM scheme used for this thesis is discussed in detail in [8-9] and the Simulink diagrams can be found in Appendix C. Figure 8 is a block diagram of the functions for each process in the SVM block.

	a	b	c	d	e
Sector I	nnn	pnn	ppn	ppp	ppn
Sector II	nnn	npn	ppn	ppp	ppn
Sector III	nnn	npn	npp	ppp	npp
Sector IV	nnn	nnp	npp	ppp	npp
Sector V	nnn	nnp	npp	ppp	nnp
Sector VI	nnn	pnn	pnp	ppp	pnp

Table 1. Space Vector Modulation Switching Pattern [From 9].

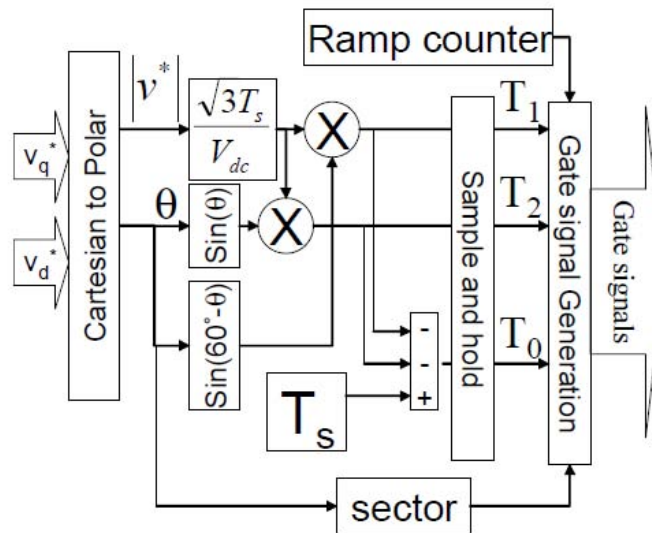


Figure 8. SVM Digital Implementation Diagram [From 8].

E. ENCODER IMPLEMENTATION

The encoder used for the DFIG rotor position and speed input is the Microtech Laboratory Inc. (MTL) MES-20-200P C. Its implementation is discussed in [10], however several modifications were made to commission the encoder in this thesis. The encoder uses a single shaft, 200 pulse, open collector output design to produce an A_k , B_k and Z_k pulse sequence as seen in Appendix A and Figure 9 (experimental Chipscope capture).

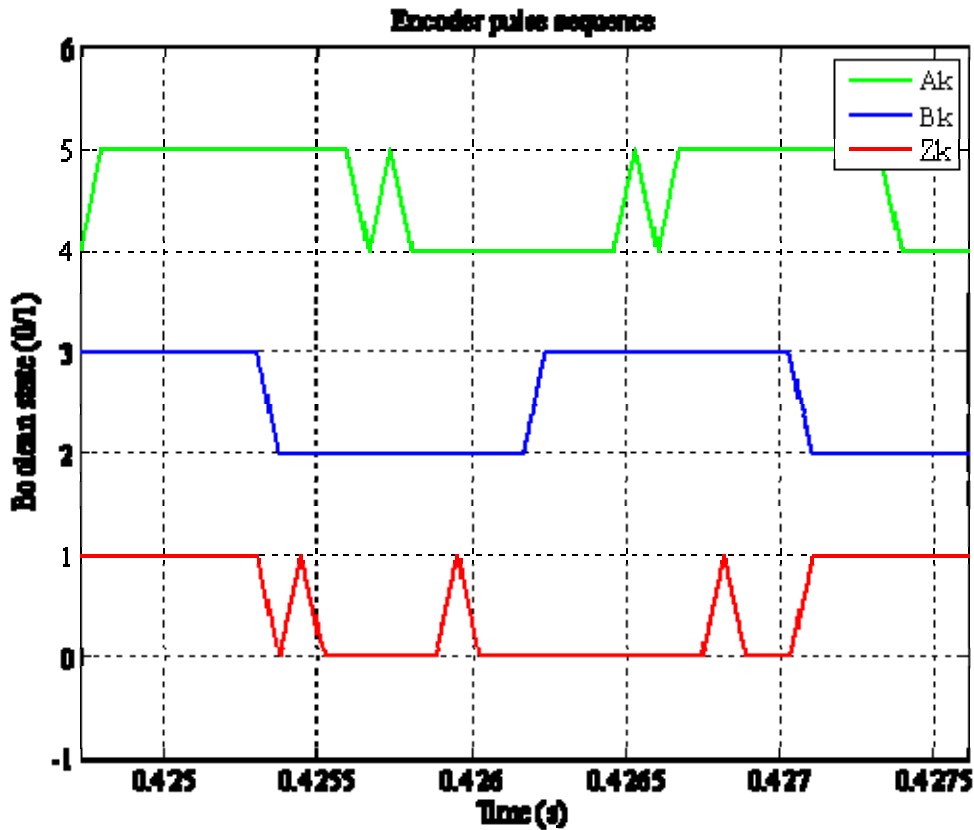


Figure 9. Experimental: Encoder A, B and Z Pulse Configuration.

Of note, the imperfections shown in Figure 9, and some subsequent figures, are caused by a Chipscope plot function artifact due to Chipscope timing discrepancies. Pulses A_k and B_k are in quadrature, and the Z_k pulse occurs once every revolution (200

pulses) in alignment with the B pulse period. In order to derive the rotor position from this encoder input a Simulink block was created to use the A_k and B_k pulses as an incremental counter and the Z_k pulse as a one revolution reset. Figure 10 is the Simulink block implemented for this function.

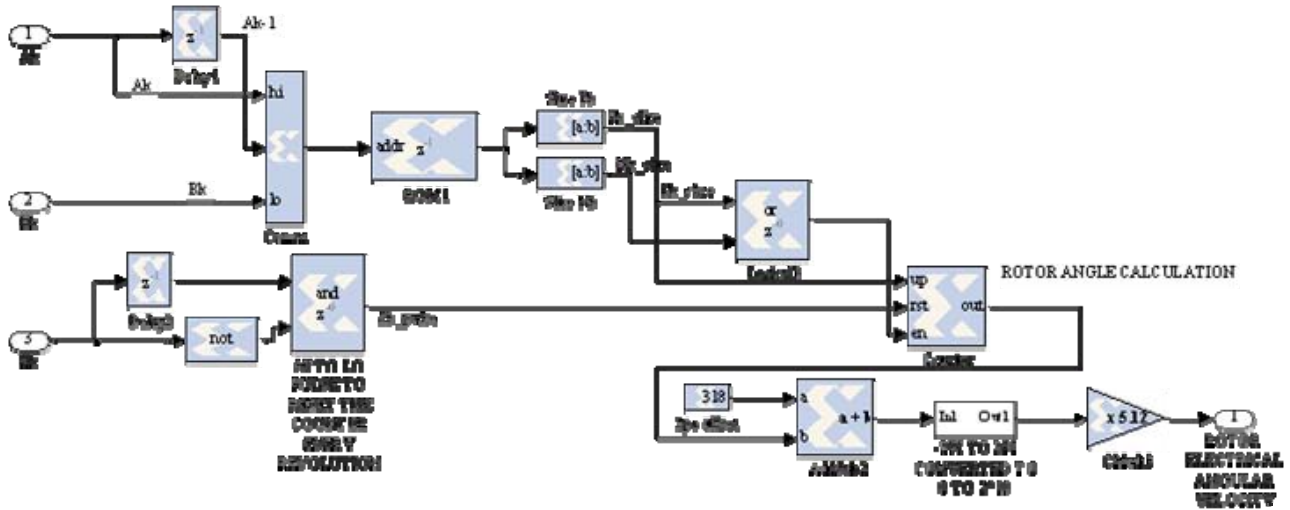


Figure 10. Architecture Used to Derive Rotor Angular Position from the Encoder.

The concatenation block takes A_k , A_{k-1} and B_k and forms a three bit word and relates it to a two bit word (P_k and N_k combined). The two bit word is compared to the predetermined encoder vector in the ROM block (P_k and N_k is also used to enable the counter). The predetermined encoder vector is specific to the encoder characteristics and is used to indicate whether the encoder shaft is turning clockwise (binary 1 0) or counter-clockwise (binary 1 1), hence count up or down. A rising and falling edge architecture is chosen for the encoder algorithm, which effectively doubles the encoder resolution from 200 triggers per revolution to 400 triggers per revolution. The two bit word is then passed through the Simulink Slice block, which separates the word into two one bit words. P_k and N_k trigger the counter to count up or down with a range of 0 to 2^{10} bits with a wrap feature triggered by the reset pulse. Table 2 shows a detailed account of the encoder algorithm.

A_k	A_{k-1}	B_k	P_k N_k (Logical OR)	Enable Up	Counter State	Encoder Vector
0	0	0	N/A	N/A	N/A	N/A
0	0	1	N/A	N/A	N/A	N/A
0	1	0	1 0	1 1	Count down	Falling edge CCW (2)
0	1	1	0 1	1 0	Count up	Falling edge CW (1)
1	0	0	0 1	1 0	Count up	Rising edge CW (1)
1	0	1	1 0	1 1	Count down	Rising edge CCW (2)
1	1	0	N/A	N/A	N/A	N/A
1	1	1	N/A	N/A	N/A	N/A

Table 2. Encoder Truth Table with Directed Actions.

The Z_k pulse provides inputs to an AND gate as seen in Figure 10. Since it occurs only once per revolution, it is straightforward to see why it is used for the counter reset. The counter output is a true account of the encoder position, however the actual rotor electrical position is not accurate until the encoder zero point is calibrated to be aligned with the rotor electrical zero point.

The encoder calibration procedure began by a detailed study of the rotors physical winding layout. The DFIG is a 4-pole, 3-phase induction machine with 24 slots and no accessible rotor windings neutral point. A simple method of aligning the rotor to a zero point electrical position would be to supply power to the phase A windings of the rotor and stator and allow the magnetizing flux to align the two. Without access to the rotor winding's neutral point, this method became moot. The second, and possibly more accurate, method to align the rotor to its zero point electrical position was to supply power to the rotor and stator phases via line-to-line. After several experiments with the line-to-line method, there were multiple convergences to a rotor zero point electrical position to be 318 triggers out of 400. This offset was added to the encoder algorithm as the calibration point. Finally, the calibrated encoder signal was passed through a series of conversions so that it corresponded to the rotor electrical angular position and also had a wrapping range of $0-2^{10}$ bits per revolution. Figure 11 shows the experimental results of the calibrated rotor electrical angular position.

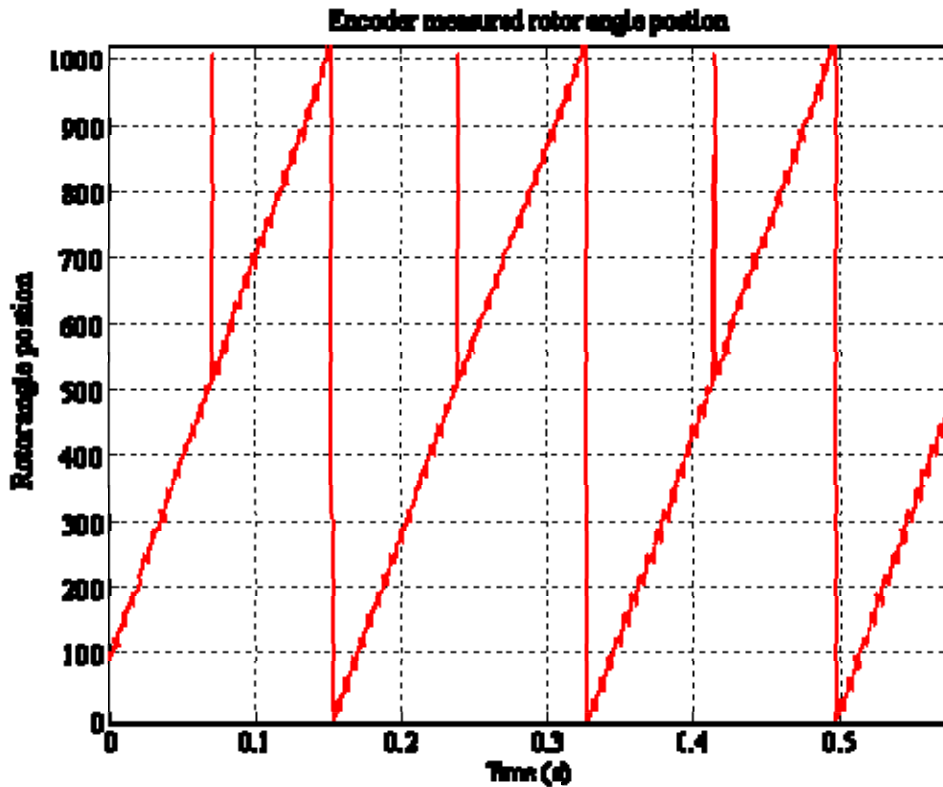


Figure 11. Experimental: Calibrated Rotor Electrical Angular Position.

The last input the encoder provided was the electrical angular frequency, w_r . This derivation was simply a differentiation of rotor electrical angular position with respect to time. Due to the limitations of Simulink's iterative features, the output of this differentiation was crude and noisy. However, after passing this output through a first order low pass filter with a corner frequency of 10Hz, the signal was surprisingly accurate and proved to be very functional for this application.

THIS PAGE INTENTIONALLY LEFT BLANK

IV. RESULTS

A. OVERVIEW

In this thesis, we emulate a Wind Turbine Generator by driving a DFIG via a DC motor with variable input torque capability. As discussed in [1-4], we can use a DFIG with back-to-back SVMs to accomplish a decoupled Supply-side, and DFIG-side, control scheme while allowing power flow to occur between the two systems.

The two circuits of concern are the DFIG and Supply-side circuits. The DFIG and Supply-side circuits are electrically coupled with back-to-back (DFIG-side and Supply-side) SVMs that are coupled through a DC Link consisting of a capacitor bank. The back-to-back SVMs, with DC Link, provide bi-directional power flow between the DFIG rotor and Supply-side power supply. Bi-directional power flow is achieved when the DFIG is controlled at supersynchronous speeds, and input torque is enough to overcome losses, and subsynchronous speeds (Supply-side provides power to rotor).

B. SUPPLY-SIDE EXPERIMENTS

The Supply-side power supply (3-phase AC) provides power to the Supply-side circuit (stepped down by a VARIAC) and the Stator of the DFIG. The Supply-side circuit senses the supply side voltage, current and DC Link voltage and sends the sensed inputs to a FPGA. The FPGA is programmed via a Simulation software package called Simulink to achieve the desired control of the specified parameters. For the Supply-side circuit we use the mentioned sensed inputs to derive control of V_{DC} so that it is maintained at 200V via SVM. There is also a built-in protection feature in the Supply-side circuit that will turn off the SVM if a VDC of 240V is reached. Within the Supply-side controller architecture, however, there are parameters that can be used to control the system power factor. The research of this feature, and its effects on the grid, was beyond the scope of this thesis, but some simulation and experimental tests were conducted to show the performance of the controller. If a system, connected to the grid, has explicit control of its power factor, it can be used to reduce transmission line losses by controlling the amount

of reactive power being distributed. Figures 12 and 13 show the simulation and experimental steady state shifts in power factor when i_{d_ref} was commanded at 2A and -2A.

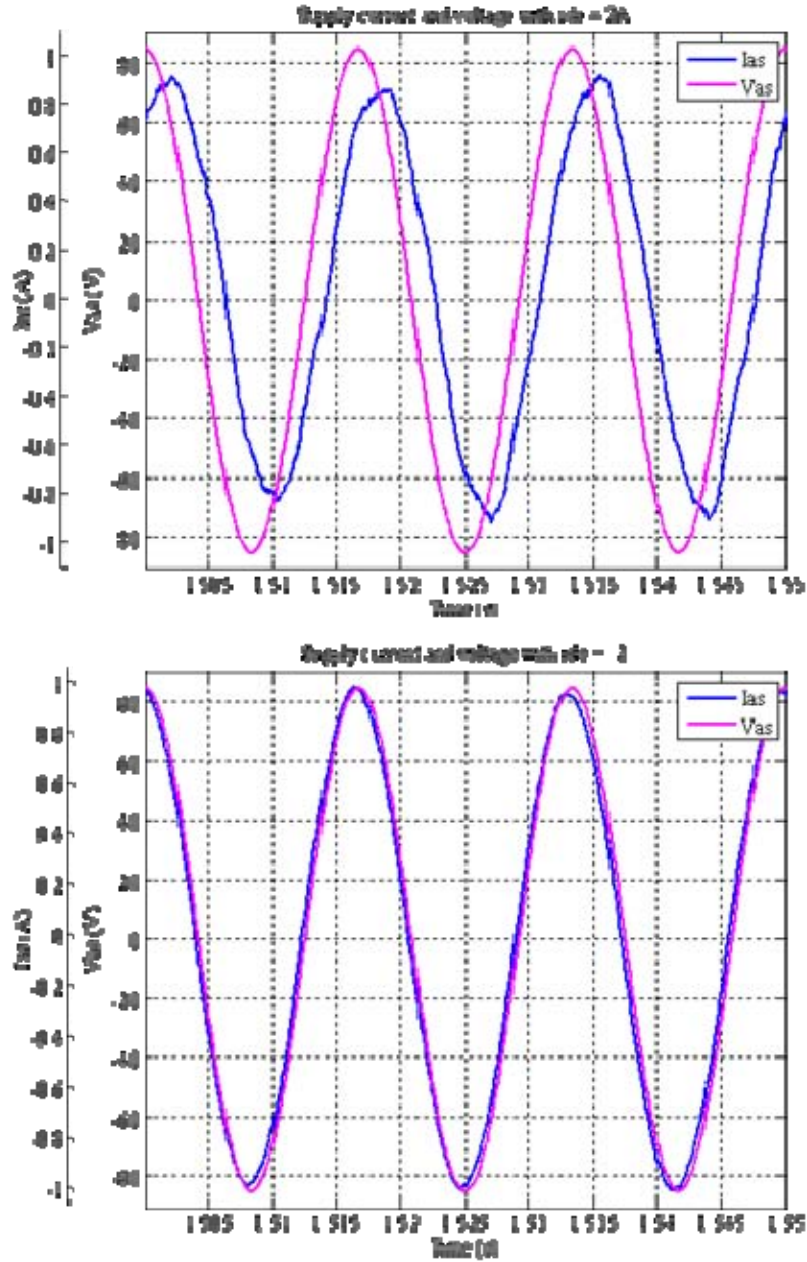


Figure 12. Simulation: Supply-side Voltage and Current with i_{d_ref} at 2A and -2A.

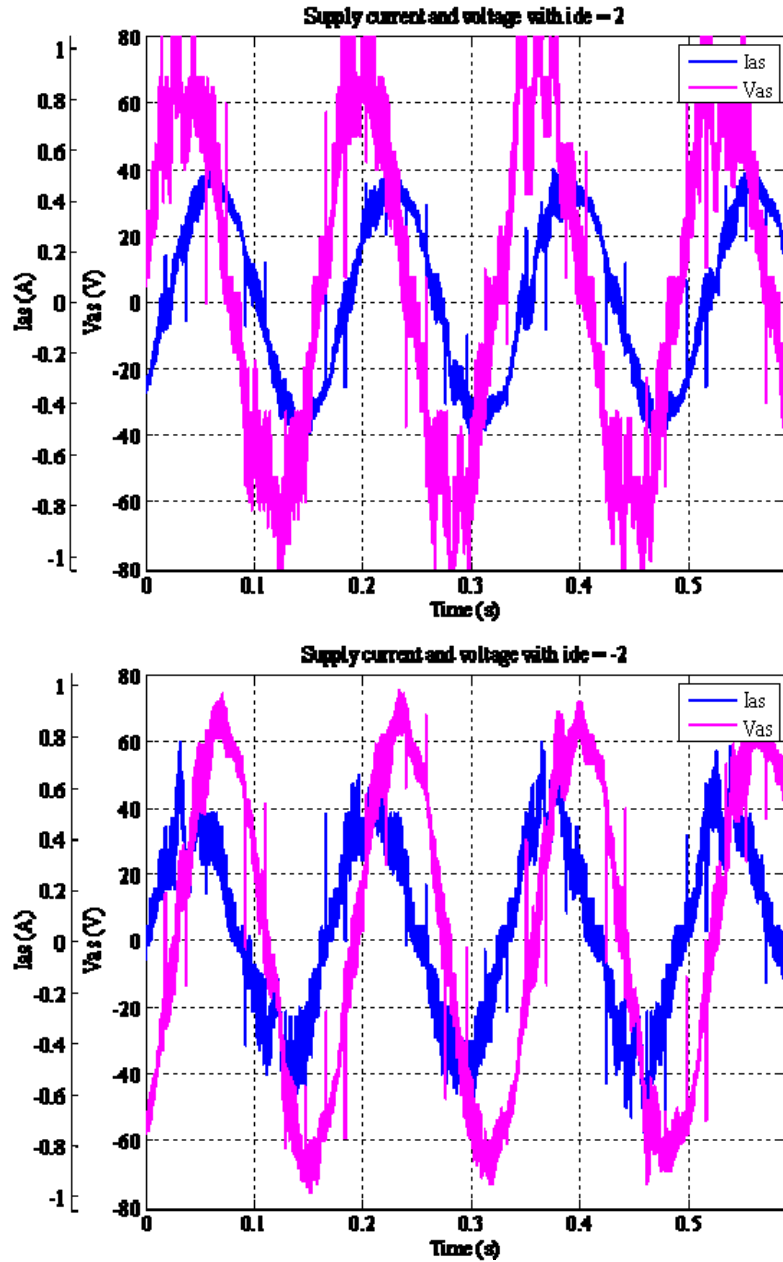


Figure 13. Experimental: Supply-side Voltage and Current with $i_{d_{ref}}$ at 2A and -2A.

C. DFIG-SIDE EXPERIMENTS

The DFIG circuit power supply is provided by the DC Link and DFIG-side SVM. The DFIG circuit senses rotor current, stator voltage, rotor speed, and rotor electrical position (as provided by an encoder). These inputs, like the Supply-side circuit, are then

sent to an FPGA, which is programmed to control the DFIG parameters. The DFIG circuit will take the rotor speed input and derive a current reference that is used to control the rotor speed using a PI controller. It is important to show that we can control the DFIG rotor speed since traditional Wind Turbine Generators would use turbine blade pitch control in tandem with a synchronous generator to provide a constant speed, and hence a constant output frequency. Further, it is noteworthy that a wind-speed profile can be adapted to a specific Wind Turbine (outfitted with a DFIG) in order to program the DFIG to run at specified speeds for a given wind speed. This tool can be used to provide an optimized rotor speed for a given wind speed. For our application we will show that the DFIG rotor speed can be controlled (subsynchronous, synchronous or supersynchronous) for any given input torque and thus distributes the power generated by the DFIG as predicted between the rotor and stator. Further, this experiment will demonstrate the bi-directional power flow of the back-to-back SVMs showing power recovery via the DFIG rotor.

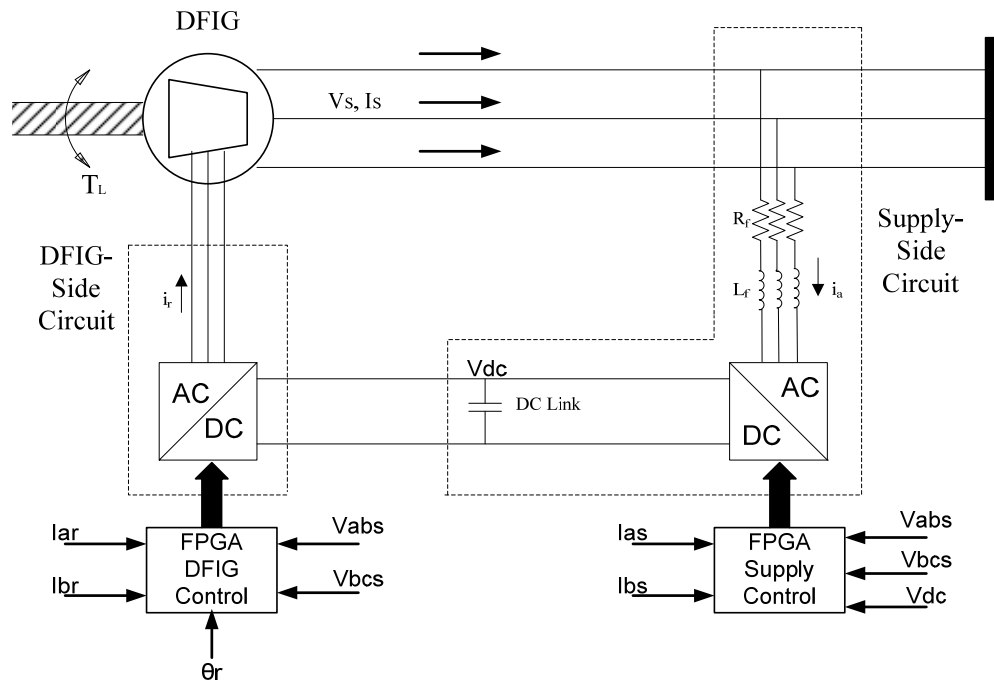


Figure 14. Simplified Circuit of Wind Turbine DFIG System.

As illustrated in Figure 14, the Supply-side SVM converts a 3-phase AC source to a constant DC Link voltage of 200V. The DC Link voltage is then inverted into a 3-phase waveform via the DFIG-Side SVM (during modes for which power is being delivered to the DFIG). The digital control for the Insulated Gate Bipolar Transistor (IGBT) network is implemented via the FPGA. The FPGA interface samples the rotor current and the stator voltage of the DFIG through an A/D converter. There is an input from the encoder, θ_r , to provide the position and speed of the rotor to the FPGA through the interface circuit board. An algorithm then calculates the slip frequency of the DFIG, which is used to derive the needed rotor current frequency and amplitude to maintain a specified rotor speed, and therefore a controllable output frequency. Since the Supply-side and DFIG-side controller topologies are nearly identical, it follows that the DFIG-side controller can control system power factor in the same way that the Supply-side did. Figures 15 and 16 show the simulation and experimental steady state shifts in power factor when i_{d_ref} was commanded at 2A and -2A.

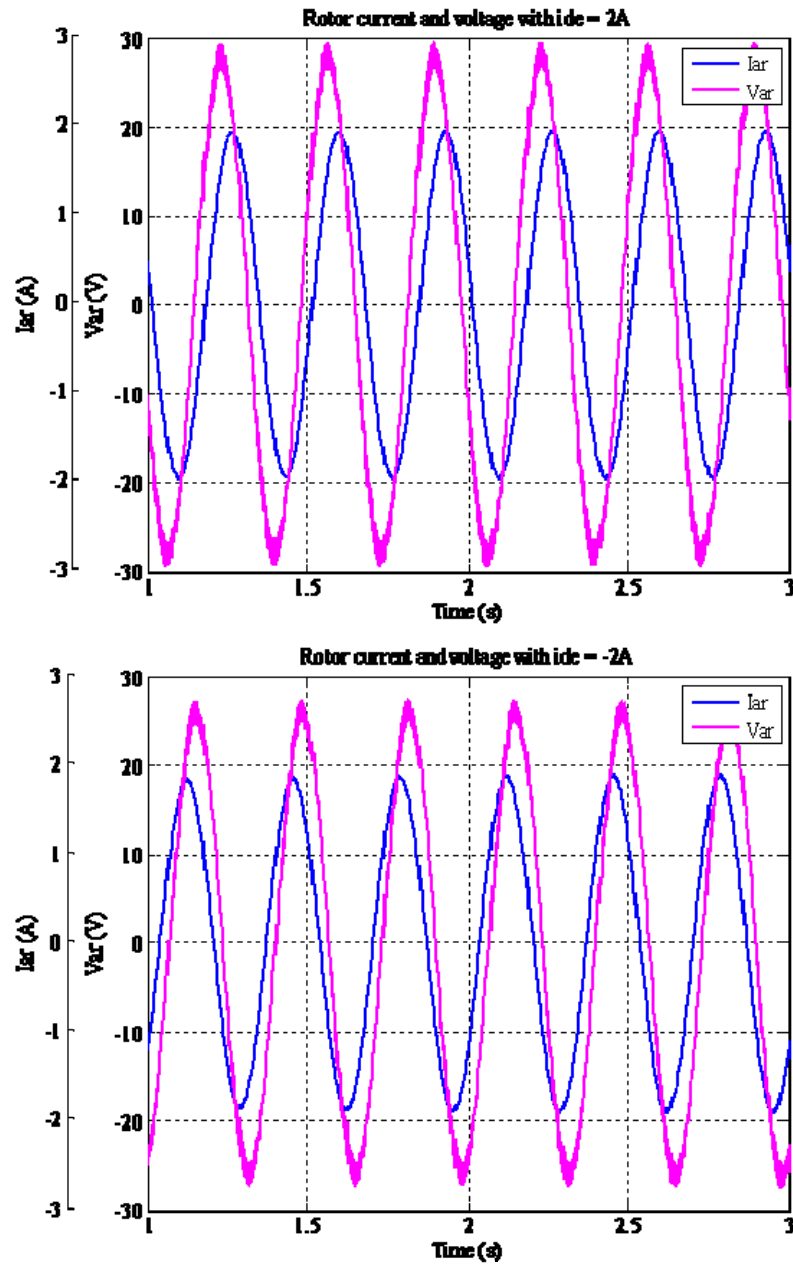


Figure 15. Simulation: DFIG-side Voltage and Current with $i_{d_{ref}}$ at 2A and -2A.

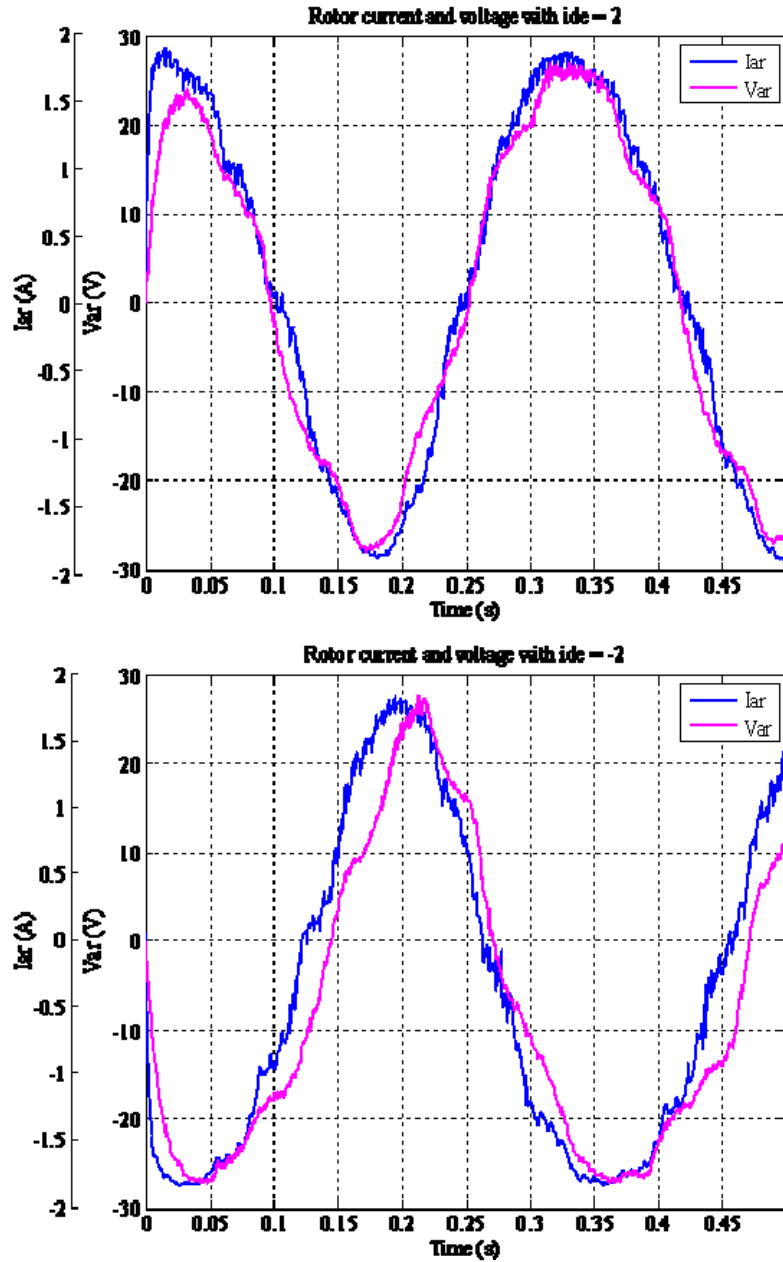


Figure 16. Experimental: DFIG-side Voltage and Current with $i_{d_{ref}}$ at 2A and -2A.

Figure 17 demonstrates an input torque transient representing a large wind gust. By commanding a specified supersynchronous speed, while taking into account windage and friction losses of the system, it is clear that the input torque transient produces a

power flow reversal in the rotor. In other words, the rotor mode transitions from power flow from the rotor (negative rotor current) to power flow to the rotor (positive rotor current).

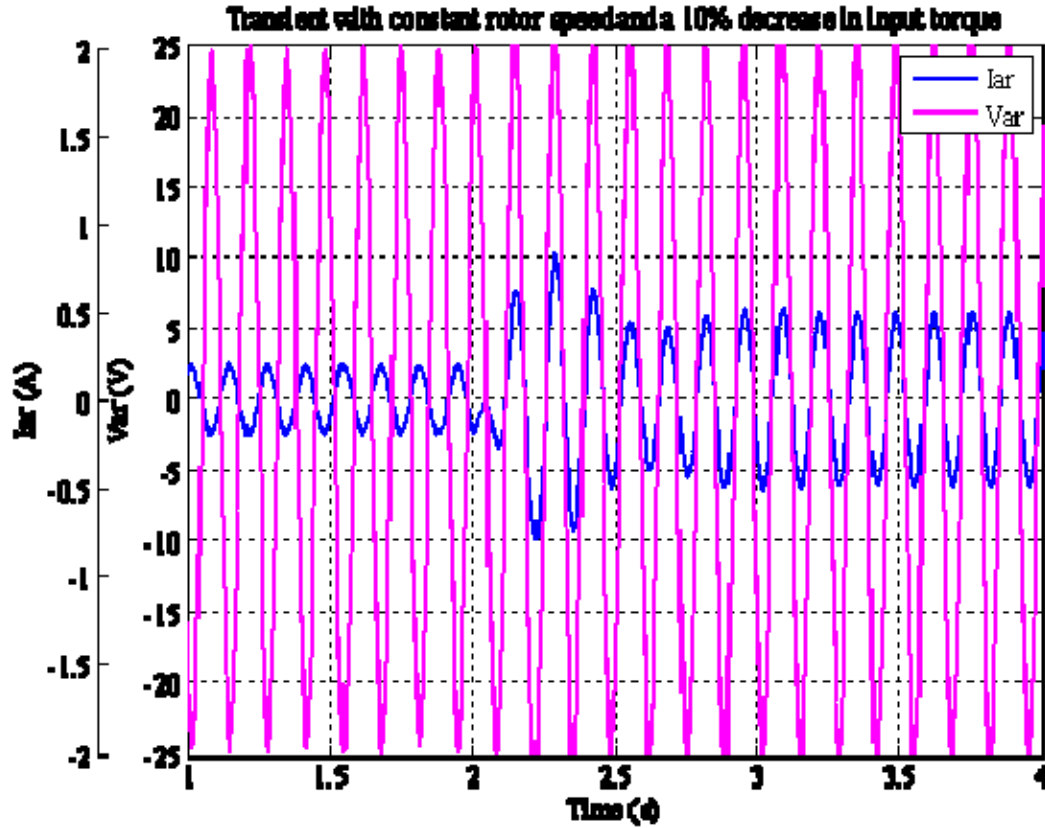


Figure 17. Simulation: Input Torque Transient Showing Rotor Power Reversal.

Figures 18 and 19 (experimental results) parallels this transition with the steady state captures corresponding to the simulation transient. The experimental results were run through a low pass filter with a corner frequency of 80 Hz in order to create a useful plot of the event. Due to windage and friction losses, a commanded supersynchronous speed was ordered to achieve the power flow transition results during the constant rotor speed experiment.

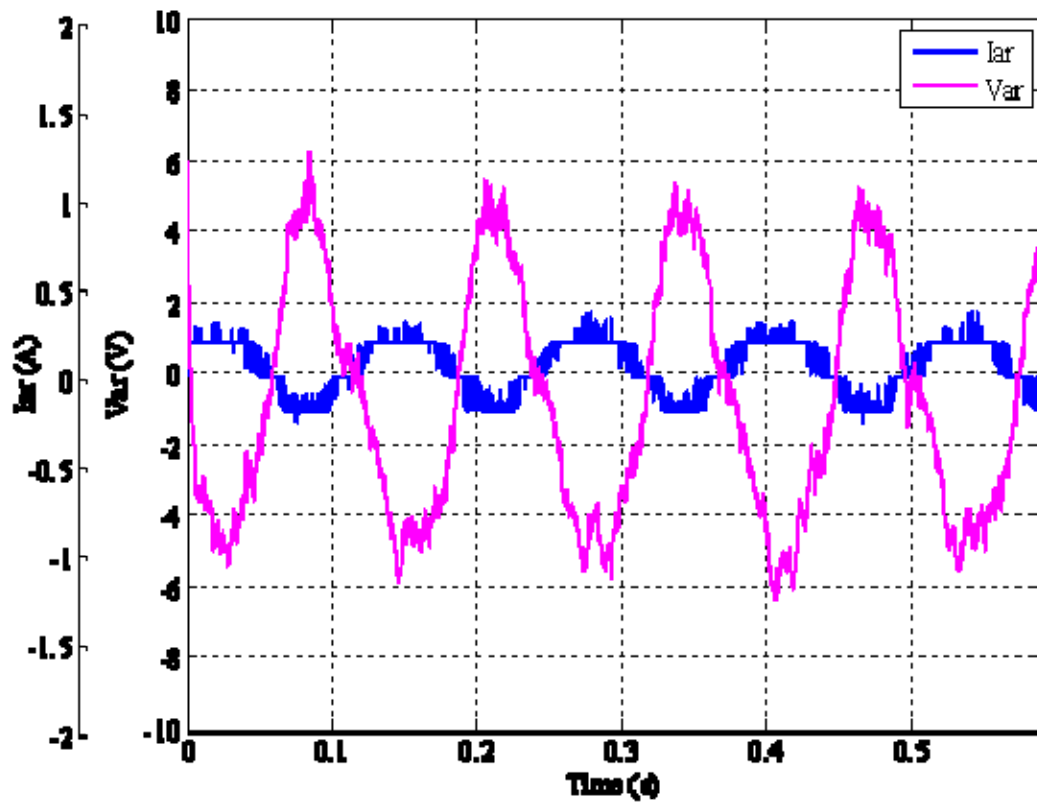


Figure 18. Experimental: Rotor Current and Voltage with Power Flow from the Rotor.

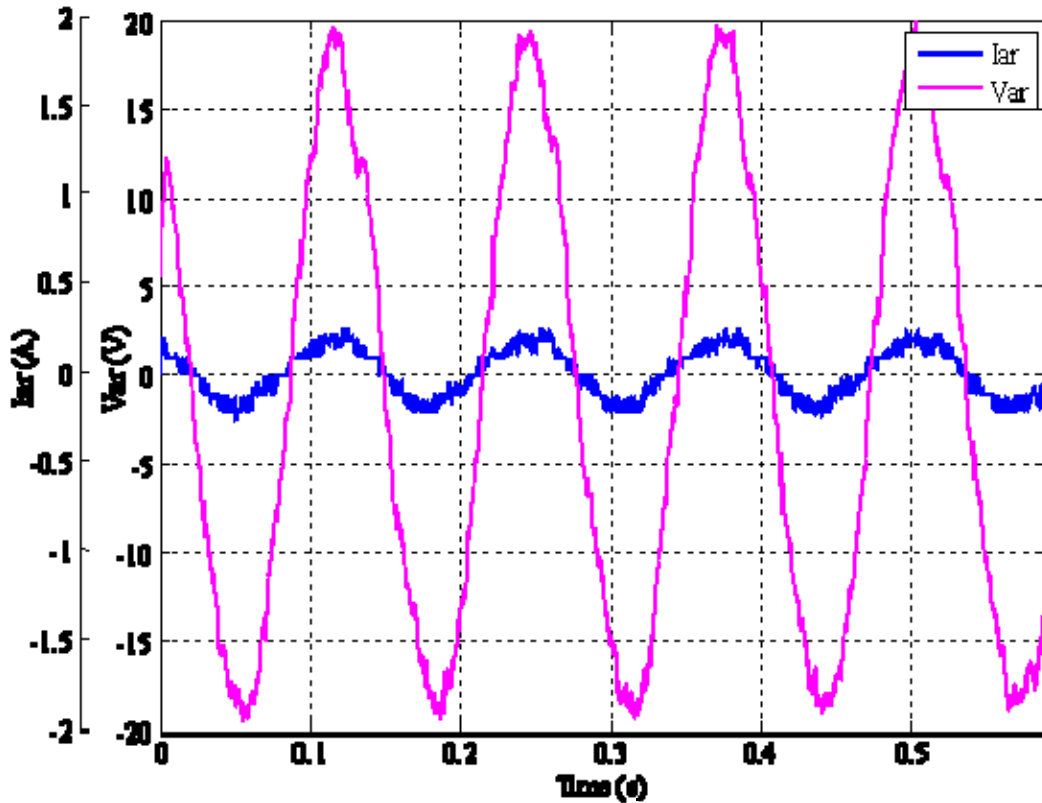


Figure 19. Experimental: Rotor Current and Voltage with Power Flow to the Rotor.

Additionally, Figure 17 (simulation model) shows a smooth transition as the power flow reverses between power flow from the rotor to power flow to the rotor. This transition is modeled using a constant commanded rotor speed along with a 10% decrease in input torque.

Figure 20 demonstrates a large, constant input torque representing a constant wind speed. By increasing the commanded rotor speed by 30%, while taking into account windage and friction losses of the system, it is clear that the rotor speed transient produces a power flow reversal in the rotor that corresponds to subsynchronous, synchronous and supersynchronous speeds. In other words, the rotor mode transitions from power flow to the rotor (positive rotor current) to power flow from the rotor (negative rotor current).

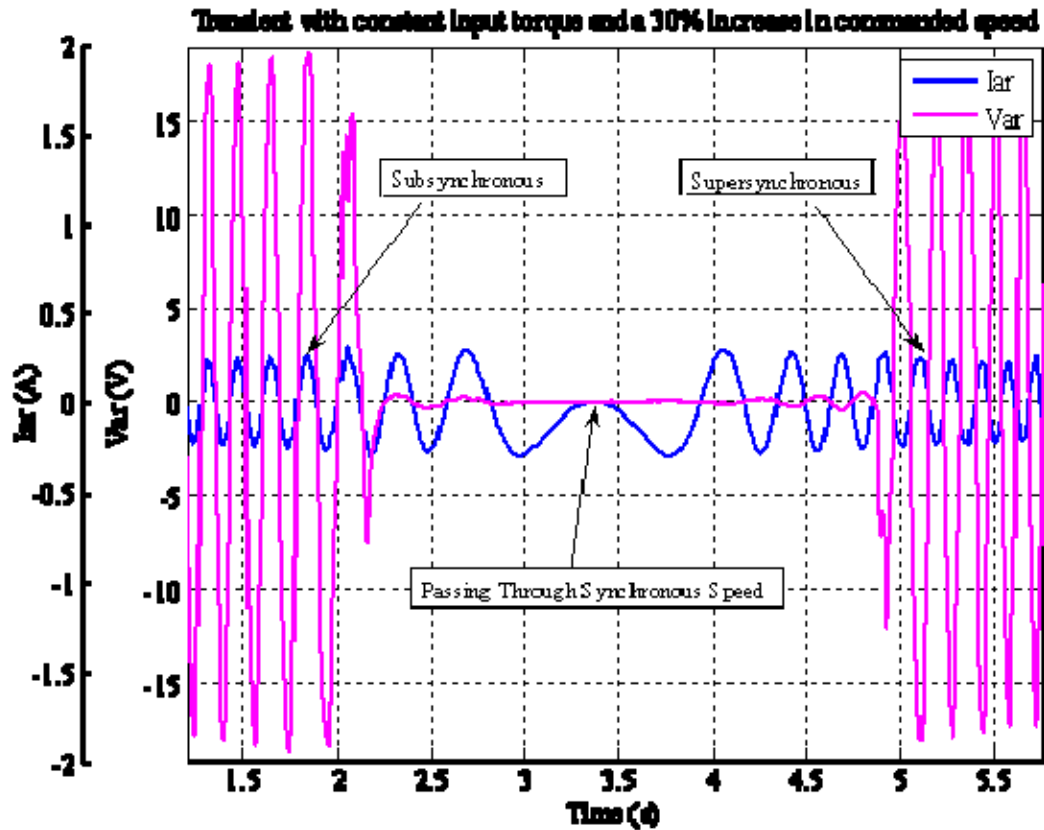


Figure 20. Simulation: Increase in Rotor Speed with a Constant Input Torque.

Figures 21 through 23 (experimental results) parallels Figure 20 with the steady state captures corresponding to the simulation transient. The experimental results were run through a low pass filter with a corner frequency of 80 Hz in order to create a useful plot of the event.

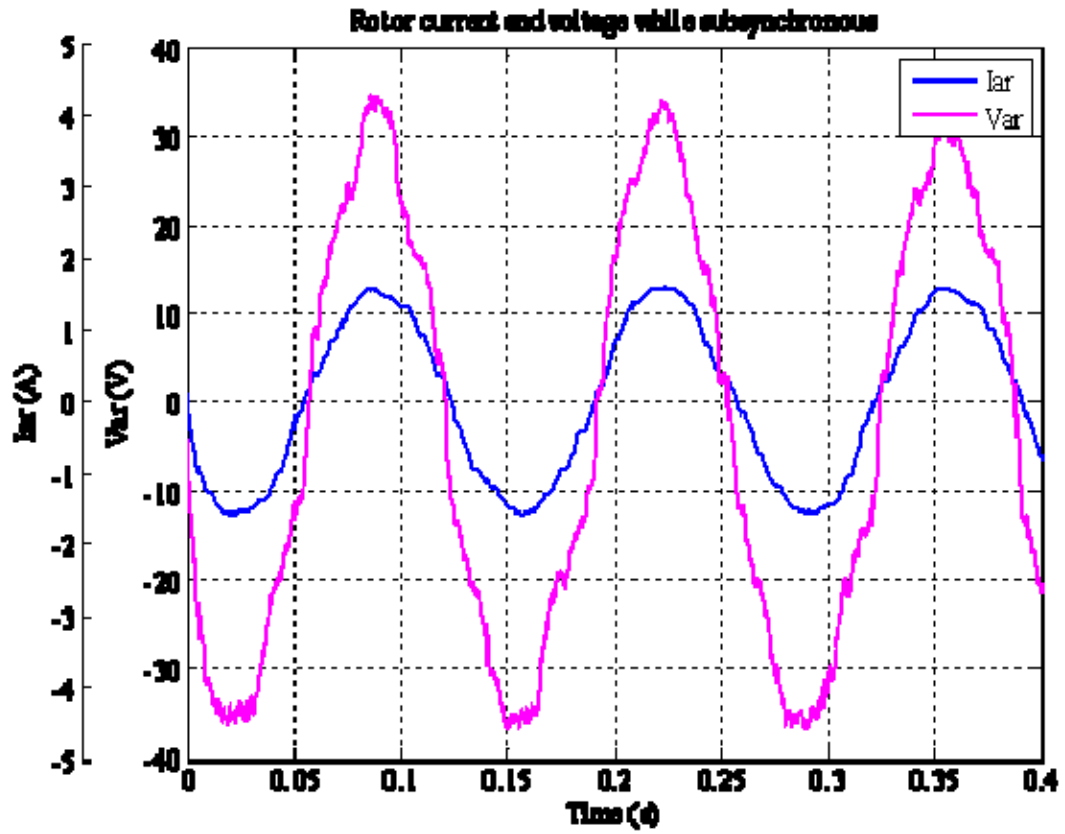


Figure 21. Experimental: Rotor Current and Voltage While Subsynchronous.

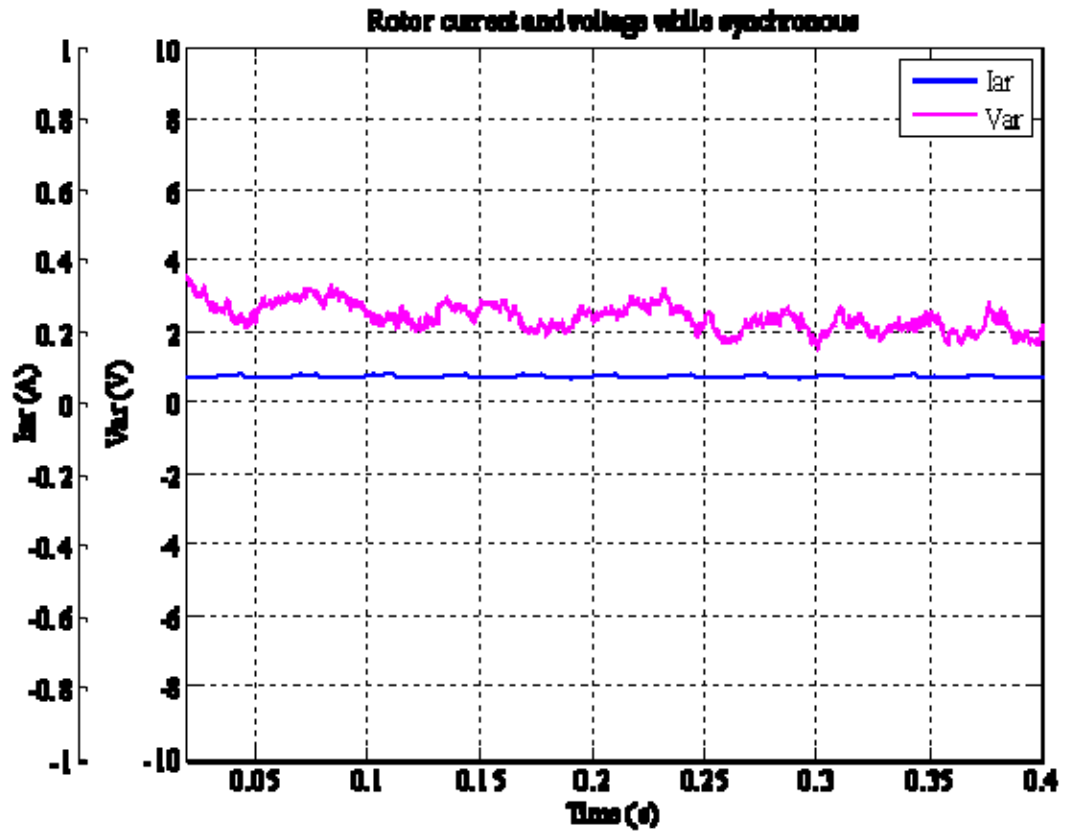


Figure 22. Experimental: Rotor Current and Voltage While Synchronous.

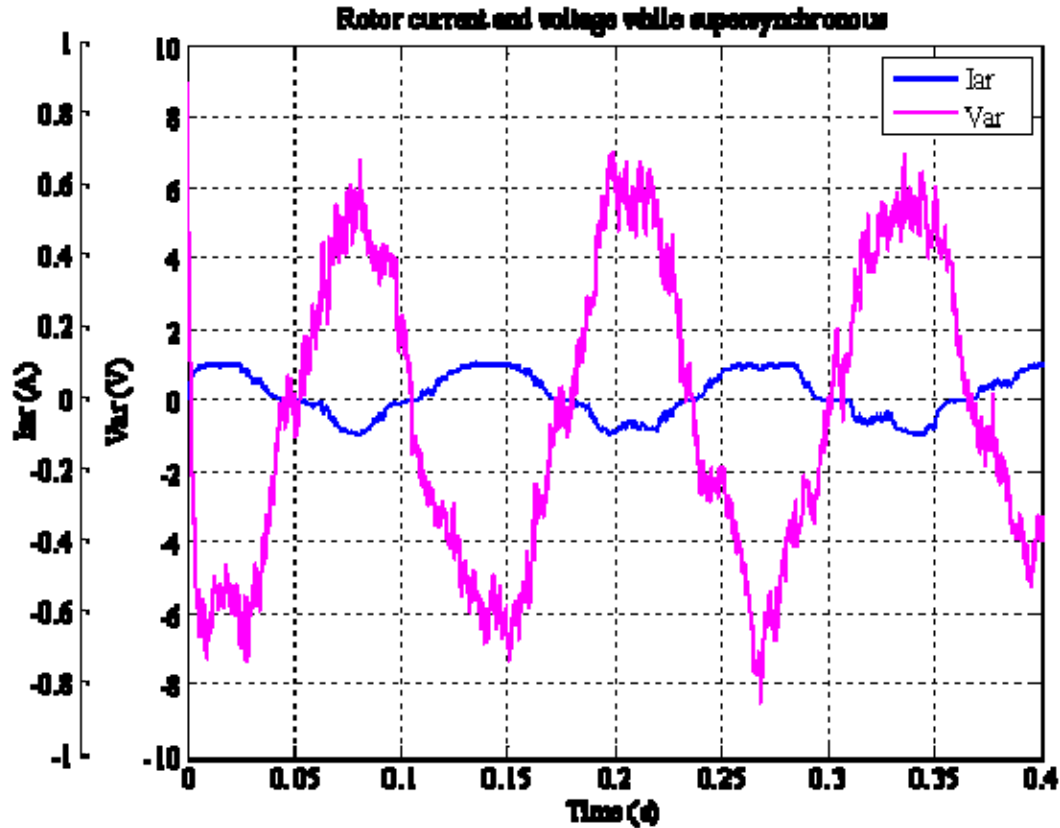


Figure 23. Experimental: Rotor Current and Voltage While Supersynchronous.

In conclusion, we showed that we can control the DFIG rotor excitation to provide a constant output frequency. Our application demonstrated that the DFIG rotor speed can be controlled (subsynchronous, synchronous or supersynchronous) for a given input torque and thus distributes the power generated by the DFIG as predicted between the rotor and stator. Finally, this experiment also demonstrates the bi-directional power flow of the back-to-back SVMs showing power recovery via the DFIG rotor.

V. CONCLUSIONS AND FUTURE RESEARCH

A. CONCLUSIONS

The Wind Turbine Power Generation Emulation via Doubly Fed Induction Generator Control System was designed, simulated, constructed and tested using standard engineering principles and theory. Since the research and simulation phases were aptly utilized, the development and construction phases were relatively inexpensive and short. A series of test were conducted and validated the design. The experimental results showed that the system responded according to the simulation.

With a baseline prototype that functions correctly, the Naval Postgraduate School now has a means to build a large scale prototype for laboratory purposes and future research. The future research on this topic will be above and beyond current publications, and will have an enabled freedom to exploit the abilities of the DFIG.

B. FUTURE RESEARCH

A third SDC should be used to take control of the DC motor. This Wind-side SDC can be programmed to mirror current wind speed profiles that are available from the National Renewable Energy Laboratory. With a wind speed profile controlling the input torque of the DFIG, the DFIG-side SDC can be slightly modified to include a rotor speed lookup table. This lookup table can be used to derive an optimal rotor speed for a given wind speed, and thus increase the efficiency of DFIG power extraction.

Second, DFIG-side feed forward terms, based on slip speed and flux linkages, can be implemented as described in [1]. The feed forward terms should lower the DFIG-side PI controller time constant without any detrimental effects on stability.

Finally, Supply-side feed forward terms, based on the stators synchronous angular frequency and stator winding inductance, can be added. Again, these terms should lower Supply-side PI controller time constants without any detrimental effects on stability.

THIS PAGE INTENTIONALLY LEFT BLANK

APPENDIX A: DATASHEETS

SEMISTACK - IGBT



SEMITRANS Stack¹⁾

Three-phase rectifier + inverter with brake chopper

SEMITEACH - IGBT
SKM 50 GB 123D
SKD 51
P3/250F

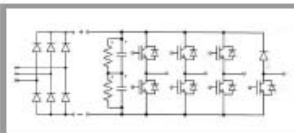
Features

- Multi-function IGBT converter
- Transparent enclosure to allow visualization of every part
- IP2x protection to minimize safety hazards
- External banana/BNC type connectors for all devices
- Integrated drive unit offering short-circuit detection/cut-off, power supply failure detection, interlock of IGBTs + galvanic isolation of the user
- Forced-air cooled heatsink

Typical Applications

- Education: One stack can simulate almost all existing industrial applications:
 - 3-phase inverter+brake chopper
 - Buck or boost converter
 - Single phase inverter
 - Single or 3-phase rectifier

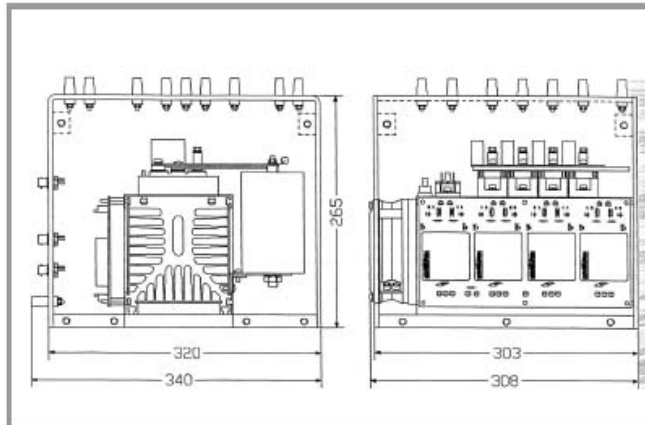
¹⁾ Photo non-contractual



B6U + B6CI + E1CIKF

Circuit	I_{rms} (A)	V_{ac} / V_{dmax}	Types
B6CI	30	440 / 750	SEMITEACH - IGBT

Symbol	Conditions	Values	Units
I_{rms}	no overload IGBT - 4x SKM 50 GB 123D	30	A
V_{CES}		1200	V
$V_{CE(SAT)}$	$I_c = 50A, V_{GE} = 15V, \text{chip level}; T_j = 25(125)^\circ C$	2,7 (3,5)	V
V_{GES}		± 20	V
I_c	$T_{case} = 25 (80)^\circ C$	50 (40)	A
I_{CM}	$T_{case} = 25 (80)^\circ C; t_p = 1ms$	100 (80)	A
$V_{in(max)}$	Rectifier - 1x SKD 51/14		
	without filter	3 x 480	V
	with filter	3 x 380	V
C_{opt}	DC Capacitor bank - Electrolytic 2x 2200 μF /400V	1100 / 800	$\mu F / V$
V_{DCmax}	total equivalent capacitance max. DC voltage applied to the capacitor bank	750	V
Power supply Current consumption	Driver - 4x SKH1 22	0 / 15	V
	max; per driver	16	mA
Thermal trip	Normally Open type (NO)	71	$^\circ C$



General dimensions

This technical information specifies semiconductor devices but promises no characteristics. No warranty or guarantee expressed or implied is made regarding delivery, performance or suitability.

Model 8231 Three-Phase Wound-Rotor Induction Motor



Each phase of the stator windings of this motor is independently terminated and identified on the faceplate to permit operation in either delta or star (wye) configuration. The rotor windings are brought out to the faceplate via external slip rings and brushes. This machine can be used as a wound-rotor induction motor, phase shifter, single-phase variable coupling transformer, three-phase transformer, selsyn control, frequency converter or asynchronous induction generator. The speed of this machine can be controlled through the use of the Three-Phase Rheostat (Model 8731).

SPECIFICATIONS

Model 8211 DC Motor/Generator		120/208 V – 60 Hz	220/380 V – 50 Hz	240/415 V – 50 Hz
Power Requirement		120/208 V	220/380 V	240/415 V
Rating	Motor Output Power	175 W		
	Generator Output Power	120 W	110 W	120 W
	Armature Voltage	120 V – DC	220 V – DC	240 V – DC
	Shunt Field Voltage	120 V – DC	220 V – DC	240 V – DC
	Full Load Speed	1800 r/min	1500 r/min	1500 r/min
	Full Load Motor Current	2.8 A	1.3 A	1.1 A
	Full Load Generator Current	1 A	0.5 A	0.5 A
Physical Characteristics	Dimensions (H x W x D)	308 x 291 x 440 mm (12.1 x 11.5 x 17.3 in)		
	Net Weight	14.1 kg (31 lb)		
Model 8221 Four-Pole Squirrel-Cage Induction Motor		120/208 V – 60 Hz	220/380 V – 50 Hz	240/415 V – 50 Hz
Power Requirement		120/208 V	220/380 V	240/415 V
Rating	Output Power	175 W		
	Stator Voltage	120/208 V, 3-phase	220/380 V, 3-phase	240/415 V, 3-phase
	Full Load Speed	1670 r/min	1360 r/min	1395 r/min
	Full Load Current	1.2 A	0.52 A	0.46 A
Physical Characteristics	Dimensions (H x W x D)	308 x 291 x 440 mm (12.1 x 11.5 x 17.3 in)		
	Net Weight	13.5 kg (29.7 lb)		
Model 8231 Three-Phase Wound-Rotor Induction Motor		120/208 V – 60 Hz	220/380 V – 50 Hz	240/415 V – 50 Hz
Power Requirement		120/208 V	220/380 V	240/415 V
Rating	Output Power	175 W		
	Stator Voltage	120/208 V, 3-phase	220/380 V, 3-phase	240/415 V, 3-phase
	Rotor Voltage	60/104 V, 3-phase	110/190 V, 3-phase	120/208 V, 3-phase
	Full Load Speed	1500 r/min	1240 r/min	1315 r/min
	Full Load Current	1.3 A	0.53 A	0.48 A
Physical Characteristics	Dimensions (H x W x D)	308 x 291 x 440 mm (12.1 x 11.5 x 17.3 in)		
	Net Weight	14 kg (30.8 lb)		



POWER SUPPLY MODEL 8821

The Power Supply provides fixed and variable AC and DC voltage sources, all terminated by color-coded 4 mm safety sockets. Independent circuit breakers, reset at the front panel, protect the input to and output from the Power Supply. Indicator lamps monitor the presence of input voltage in each phase. When a phase leg of the site's power service is out, the lamp goes off to reflect this condition.

A voltmeter, connected through a selector switch, monitors the variable AC and DC outputs and fixed DC output. A 24 V AC output provides a low-voltage supply required to operate other EMS equipment such as metering modules and modules used in the Power Electronics Training System.

SPECIFICATIONS

Model 8821 – Power Supply		120/208 V – 60 Hz	220/380 V – 50 Hz	240/415 V – 50 Hz
Input	Line Voltage	120/208 V	220/380 V	240/415 V
	Line Current	15 A	10 A	
	Service Installation	20 A, 3-phase, 5 wires, star (Wye)- connected, including neutral and ground		
Outputs	Fixed AC 3-Phase	120/208 V – 15 A	220/380 V – 10 A	240/415 V – 10 A
	Variable AC 3-Phase	0-120/208 V – 5 A	0-220/380 V – 3 A	0-240/415 V – 3 A
	Variable DC	0-120 V – 8 A	0-220 V – 5 A	0-240 V – 5 A
	Fixed DC	120 V – 2 A	220 V – 1 A	240 V – 1 A
	Low Power AC	24 V – 3 A		
Wall Outlet included	NEMA L21-20	NEMA L22-20	CLIPSAL 56SO520	
Power Cord	3 m (10 ft)			
Physical Characteristics	Dimensions (H x W x D)	308 x 287 x 500 mm (12.1 x 11.3 x 19.7 in)		
	Net Weight	18.4 kg (40.5 lb)		

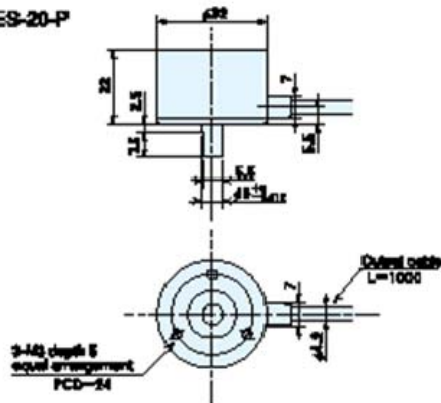
ME-20-P series

[Square Wave/Incremental]

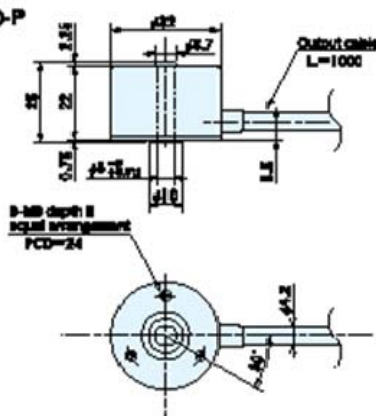


Outside dimensions

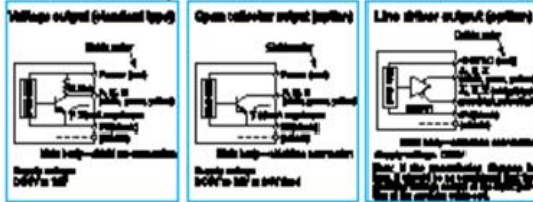
ME-20-P



MEH-20-P



Output circuit diagram

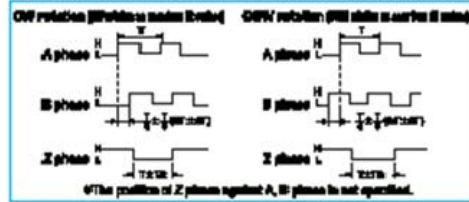


A resistor (R_L) is connected between OV and FB (phase ground).

Specifications

Type name	ME-20-P																																																													
Item	<table border="1"> <tr> <th>Unit</th> <th>Part</th> <th>Output</th> </tr> <tr> <td>Supply voltage</td> <td>DCV</td> <td>12V</td> </tr> <tr> <td>Current</td> <td>60mA</td> <td>or less (under no load)</td> </tr> <tr> <td>Output pulse number (Pulse number/revolution)</td> <td>40, 80, 100, 200, 300, 500, 600, 1,000, 1,500, 2,000, 3,000, 4,000, 5,000</td> <td></td> </tr> <tr> <td>Output phase</td> <td>A, B, Z</td> <td></td> </tr> <tr> <td>Output wave</td> <td>Square wave</td> <td></td> </tr> <tr> <td>Output capacity</td> <td>Sink current: 20mA Resistive voltage: 0.5V or less (at 10mA)</td> <td></td> </tr> <tr> <td>Minimum response frequency (response pulse number)</td> <td>100Hz</td> <td></td> </tr> <tr> <td>Output phase difference</td> <td>A, B phase difference: 90° ± 0.5° (T_{PCD}: T_{PCD}) Z phase T_Z: T_Z (see Output Waveform)</td> <td></td> </tr> <tr> <td>Maximum shaft load</td> <td>Eye or less (output cable 1m or less)</td> <td></td> </tr> <tr> <td>Starting torque</td> <td>2x10⁻³ N·m (0.02 kgf·cm) or less</td> <td></td> </tr> <tr> <td rowspan="2">Maximum load at shaft (standard)</td> <td>Radial</td> <td>19.0N (1.9kg)</td> </tr> <tr> <td>Tanget</td> <td>9.0N (0.9kg)</td> </tr> <tr> <td>Maximum allowable revolutions</td> <td>8,000/min</td> <td></td> </tr> <tr> <td rowspan="2">Starting ambient temperature/humidity</td> <td></td> <td>-10°C ~ 70°C</td> </tr> <tr> <td></td> <td>70%RH ~ 85%RH (no dewing)</td> </tr> <tr> <td>Storage ambient temperature</td> <td>-20°C ~ 60°C</td> <td></td> </tr> <tr> <td>Vibration resistance</td> <td>Durability: 50Hz, double amplitude 1.5mm 2 hours each in X, Y, and Z directions</td> <td></td> </tr> <tr> <td>Impact resistance</td> <td>Durability: 500m/s² (about 50G) 3 times each in X, Y, and Z directions</td> <td></td> </tr> <tr> <td>Cable</td> <td>Output diameter: 4.2 B-core vinyl wire Insulated shield cable (length 1m)</td> <td></td> </tr> <tr> <td>Mass</td> <td>70g</td> <td></td> </tr> </table>	Unit	Part	Output	Supply voltage	DCV	12V	Current	60mA	or less (under no load)	Output pulse number (Pulse number/revolution)	40, 80, 100, 200, 300, 500, 600, 1,000, 1,500, 2,000, 3,000, 4,000, 5,000		Output phase	A, B, Z		Output wave	Square wave		Output capacity	Sink current: 20mA Resistive voltage: 0.5V or less (at 10mA)		Minimum response frequency (response pulse number)	100Hz		Output phase difference	A, B phase difference: 90° ± 0.5° (T _{PCD} : T _{PCD}) Z phase T _Z : T _Z (see Output Waveform)		Maximum shaft load	Eye or less (output cable 1m or less)		Starting torque	2x10 ⁻³ N·m (0.02 kgf·cm) or less		Maximum load at shaft (standard)	Radial	19.0N (1.9kg)	Tanget	9.0N (0.9kg)	Maximum allowable revolutions	8,000/min		Starting ambient temperature/humidity		-10°C ~ 70°C		70%RH ~ 85%RH (no dewing)	Storage ambient temperature	-20°C ~ 60°C		Vibration resistance	Durability: 50Hz, double amplitude 1.5mm 2 hours each in X, Y, and Z directions		Impact resistance	Durability: 500m/s ² (about 50G) 3 times each in X, Y, and Z directions		Cable	Output diameter: 4.2 B-core vinyl wire Insulated shield cable (length 1m)		Mass	70g	
Unit	Part	Output																																																												
Supply voltage	DCV	12V																																																												
Current	60mA	or less (under no load)																																																												
Output pulse number (Pulse number/revolution)	40, 80, 100, 200, 300, 500, 600, 1,000, 1,500, 2,000, 3,000, 4,000, 5,000																																																													
Output phase	A, B, Z																																																													
Output wave	Square wave																																																													
Output capacity	Sink current: 20mA Resistive voltage: 0.5V or less (at 10mA)																																																													
Minimum response frequency (response pulse number)	100Hz																																																													
Output phase difference	A, B phase difference: 90° ± 0.5° (T _{PCD} : T _{PCD}) Z phase T _Z : T _Z (see Output Waveform)																																																													
Maximum shaft load	Eye or less (output cable 1m or less)																																																													
Starting torque	2x10 ⁻³ N·m (0.02 kgf·cm) or less																																																													
Maximum load at shaft (standard)	Radial	19.0N (1.9kg)																																																												
	Tanget	9.0N (0.9kg)																																																												
Maximum allowable revolutions	8,000/min																																																													
Starting ambient temperature/humidity		-10°C ~ 70°C																																																												
		70%RH ~ 85%RH (no dewing)																																																												
Storage ambient temperature	-20°C ~ 60°C																																																													
Vibration resistance	Durability: 50Hz, double amplitude 1.5mm 2 hours each in X, Y, and Z directions																																																													
Impact resistance	Durability: 500m/s ² (about 50G) 3 times each in X, Y, and Z directions																																																													
Cable	Output diameter: 4.2 B-core vinyl wire Insulated shield cable (length 1m)																																																													
Mass	70g																																																													

Output waveform

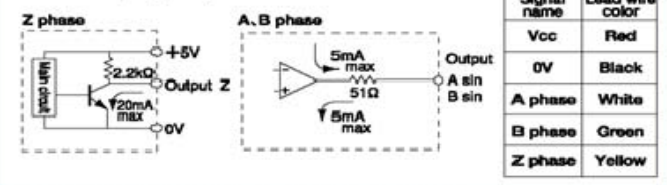


Specifications/Sine wave

Supply voltage	DC5V ±5%		
Current consumption	40mA or less (under no load)		
Detection system	Sine wave·Incremental		
Output	Output pulse number (Standard) [Pulse number/rotation]	1,000 2,000 2,500	
	Output phase	A, B, Z phase	
	Output form	A, B phase SIN wave, Z phase square wave	
	A, B, Z phase output	SIN wave 1.5 Vp-p±0.3 V offset 2.0V±0.2V	
		Opamp output current 5mA Max.	
		Harmonic distortion factor to be within 10% (Measuring condition to be within 20 kHz, effective value mean distortion factor measuring instrument)	
Maximum response frequency	50kHz		
Output phase difference	A, B phase difference 90°±45° (T/4±T/8) Z phase T±T/2 (see Output Waveform)		
Starting torque	2×10 ⁻³ N·m (20gf·cm) or less		
Allowable load of shaft (electrical)	Radial	14.7N (1.5kgf)	
	Thrust	4.9N (0.5kgf)	
Maximum allowable revolutions (mechanical)	6,000r/min		
Working ambient temperature/humidity	0°C~50°C RH35%~90% no dewing		
Storing ambient temperature	-20°C~80°C		
Vibration resistance	Durability 55Hz, double amplitude 1.5mm 2 hours each in X, Y, and Z directions		
Impact resistance	Durability 500m/s ² (about 50G) 3 times each in X, Y, and Z directions		
Cable	Outside diameter φ4.2 5-core vinyl wire Insulated shield cable (length 1m)		
Mass	70g		

Output circuit diagram

Sine wave output (option)

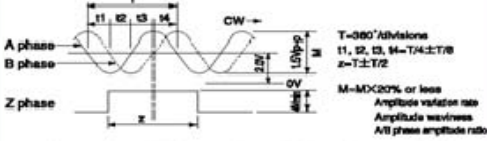


A capacitor (0.1μF) is connected between 0V and FG (frame ground).

Output waveform

Sine wave output (option)

CW rotation (CW rotation as seen from fit surface)



Specifications Built-in multiplication circuit (X2·X4·X8·X16)

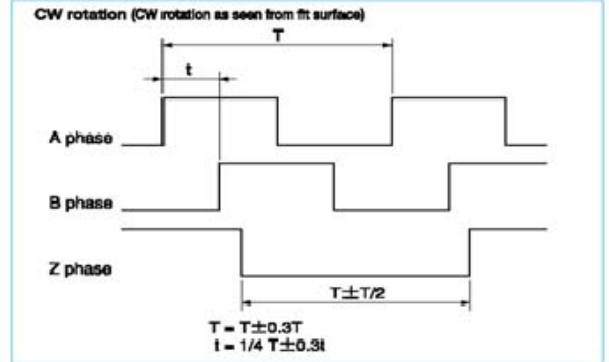
Supply voltage	Voltage/Open collector:DC5V-5%~12V+10% Line driver:DC5V±5%	
Current consumption	60mA or less (under no load)	
Detection system	Incremental	
Output	Output pulse number (Standard) [Pulse number/rotation]	EX 2,500×2 (5,000) 2,500×4 (10,000) 2,500×8 (20,000) 2,500×16 (40,000)
	Output phase	A, B, Z phase
	Output form	Square wave
	Output capacity	Open collector out put:load voltage DC13.2V max
	Maximum response frequency	Line driver output:50kHzX (by multiplication) Voltage output·Open collector output:100kHz
	Output phase difference	See the diagram below.
Starting torque	2×10 ⁻³ N·m (20gf·cm) or less	
Allowable load of shaft (electrical)	Radial	14.7N (1.5kgf)
	Thrust	4.9N (0.5kgf)
Maximum allowable revolutions (mechanical)	6,000r/min	
Working ambient temperature/humidity	-10°C~70°C RH35%~90% no dewing	
Storing ambient temperature	-20°C~80°C	
Vibration resistance	Durability 55Hz, double amplitude 1.5mm 2 hours each in X, Y, and Z directions	
Impact resistance	Durability 500m/s ² (about 50G) 3 times each in X, Y, and Z directions	
Cable	Outside diameter φ4.2 5-core vinyl wire Insulated shield cable (length 1m)	
Mass	70g	

Output circuit diagram



A capacitor (0.1μF) is connected between 0V and FG (frame ground).

Output waveform



THIS PAGE INTENTIONALLY LEFT BLANK

APPENDIX B: MATLAB M-FILES

A. MATLAB INITIAL CONDITIONS FILE

DFIG.m

```
Vdc=200;          %%%DC Link Voltage Setpoint
V_phase=sqrt(2)*120; %%%Supply-side voltage
Ks=2/3*[1 -1/2 -1/2;0 -sqrt(3)/2 sqrt(3)/2;1/2 1/2 1/2]; %abc to qd0
transformation in the stationary frame
f_fund = 60;      %%%base frequency
omega_b = 2*pi*60; %%%wr
oversample=2;    %%%VSM oversample

step_ct=1;
pulsect=1800/step_ct;
clock_freq=25e6; %%%clock frequency
tstep = 40e-9*step_ct; %%%step size
tstop=4;

%%%%%%%%%%%%%%%%%%%%%%%%%%%%%%%%%%%%%%%%%%%%%%%%%%%%%%%%%%%%%%%%%%%%%%%%%%
%%Stator PI Gains%%%%%%%%%%%%%%%%%%%%%%%%%%%%%%%%%%%%%%%%%%%%%%%%%%%%%%%%%%%%%%%%%%%%%%%%%%
Kp_vdc=.1;
Ki_vdc=10;

Kp_i_s=10;
Ki_i_s=20;

Ki_i_s_icq=0;
Ki_i_s_icd=0;
%%%%%%%%%%%%%%%%%%%%%%%%%%%%%%%%%%%%%%%%%%%%%%%%%%%%%%%%%%%%%%%%%%%%%%%%%%

Lf=300e-6;      %%%choke inductor
Rf=.05;

Amat_indI = -inv([Lf -Lf;Lf Lf+Lf])*Rf*[1 -1;1 2];
Bmat_indI = -inv([Lf -Lf;Lf Lf+Lf]);
Cmat_indI = [1 0 ;0 1 ;-1 -1 ]; %Ic = -Ia-Ib
Dmat_indI = zeros(3,2);

one_zero_state=0; %Set to one so that only one zero state is used
in modulation
if one_zero_state == 1
    gain1 = 1;
    gain2 = 0;
else
    gain1 = 1/2;
    gain2 = 1;
end

twopi3 = 2*pi/3;
```

```

poles = 4;
polesby2J=poles/2/(.089);
TL=200/(2/poles*omega_b);    %%DFIG base torque calculation

%%%%%%%%%%%%%%%%%%%%%%%%%%%%%%%%%%%%%%%%%%%%%%%%%%%%%%%%%%%%%%%%%%%%%%%%%Rotor Speed/Current PI Gains%%%%%%%%%%%%%%%%%%%%%%%%%%%%%%%%%%%%%%%%%%%%%%%%%%%%%%%%%%%%%%%%%%%%%%%%%
Kp_i=80;
Ki_i=100;

Kpgain_speed=.0333;
Kigain_speed=.0033;
%%%%%%%%%%%%%%%%%%%%%%%%%%%%%%%%%%%%%%%%%%%%%%%%%%%%%%%%%%%%%%%%%%%%%%%%%

rs=12;                %%stator res
rr = 4;                %%rotor res
Xls =9;
Xm =180;
Xlr = 9;

D=(Xls+Xm)*(Xlr+Xm)-Xm^2;
rsbyXls = rs/Xls;
rrbyXlr = rr/Xlr;
Xaq = 1/(1/Xm+1/Xls+1/Xlr);
Xad = Xaq;
XaqbyXls = Xaq/Xls;
XaqbyXlr = Xaq/Xlr;
XadbyXls = Xad/Xls;
XadbyXlr = Xad/Xlr;
XaqbyXm = Xaq/Xm;
XadbyXm = Xad/Xm;
psi_qsic=0;
psi_dsic=0;
psi_qric=0;
psi_dric=0;
omegar_ic = omega_b;
Kp_iqs=50;
Ki_iqs=.1;
Kp_iqr=50;
Ki_iqr=.1;
F_mat = [0 0 0 1;1 1 2 0;2 2 3 0;3 3 0 0];
O_mat = F_mat;

%%%%%%%%%%%%%%%%%%%%%%%%%%%%%%%%%%%%%%%%%%%%%%%%%%%%%%%%%%%%%%%%%%%%%%%%%Encoder Speed%%%%%%%%%%%%%%%%%%%%%%%%%%%%%%%%%%%%%%%%%%%%%%%%%%%%%%%%%%%%%%%%%%%%%%%%%
Vector%%%%%%%%%%%%%%%%%%%%%%%%%%%%%%%%%%%%%%%%%%%%%%%%%%%%%%%%%%%%%%%%%%%%%%%%%
Index=[1:2^12];
reciprocal=2^-6./Index;

%%%%%%%%%%%%%%%%%%%%%%%%%%%%%%%%%%%%%%%%%%%%%%%%%%%%%%%%%%%%%%%%%%%%%%%%%Encoder%%%%%%%%%%%%%%%%%%%%%%%%%%%%%%%%%%%%%%%%%%%%%%%%%%%%%%%%%%%%%%%%%%%%%%%%%
Vector%%%%%%%%%%%%%%%%%%%%%%%%%%%%%%%%%%%%%%%%%%%%%%%%%%%%%%%%%%%%%%%%%%%%%%%%%
output_vec=[0;...
            0;...
            2;...%Motor is turning in the CCW falling edge
            1;...%Motor is turning in the CW falling edge

```

```
1;...%Motor is turning in the CW rising edge
2;...%Motor is turning in the CCW rising edge
0;...
0];
%%%%%%%%%%%%%%%%%%%%%%%%%%%%%%%%%%%%%%%%%%%%%%%%%%%%%%%%%%%%%%%%%%%%%%%%
%%%
```

B. MATLAB M-FILE USED FOR SPACE VECTOR MODULATION

cverflow3.m

```
function [sector1, sector2, sector3, sector4, sector5, sector6, z] =
overflow3(x)
%gain = xfix({xlUnsigned,10,7},2.359296/3);%for 60 hz
gain = xfix({xlUnsigned,10,7},2.359296);%for 180 hz
%tempv=gain*x;
tempv=x;
if tempv<=171-1
    sector1=xfix({xlBoolean},1);
    sector2=xfix({xlBoolean},0);
    sector3=xfix({xlBoolean},0);
    sector4=xfix({xlBoolean},0);
    sector5=xfix({xlBoolean},0);
    sector6=xfix({xlBoolean},0);
    z=xfix({xlUnsigned,10,0},tempv);
elseif tempv<=2*171-1
    sector1=xfix({xlBoolean},0);
    sector2=xfix({xlBoolean},1);
    sector3=xfix({xlBoolean},0);
    sector4=xfix({xlBoolean},0);
    sector5=xfix({xlBoolean},0);
    sector6=xfix({xlBoolean},0);
    z=xfix({xlUnsigned,10,0},tempv-171);
elseif tempv<=3*171-1
    sector1=xfix({xlBoolean},0);
    sector2=xfix({xlBoolean},0);
    sector3=xfix({xlBoolean},1);
    sector4=xfix({xlBoolean},0);
    sector5=xfix({xlBoolean},0);
    sector6=xfix({xlBoolean},0);
    z=xfix({xlUnsigned,10,0},tempv-2*171);
elseif tempv<=4*171-1
    sector1=xfix({xlBoolean},0);
    sector2=xfix({xlBoolean},0);
    sector3=xfix({xlBoolean},0);
    sector4=xfix({xlBoolean},1);
    sector5=xfix({xlBoolean},0);
    sector6=xfix({xlBoolean},0);
    z=xfix({xlUnsigned,10,0},tempv-3*171);
elseif tempv<=5*171-1
    sector1=xfix({xlBoolean},0);
    sector2=xfix({xlBoolean},0);
    sector3=xfix({xlBoolean},0);
    sector4=xfix({xlBoolean},0);
    sector5=xfix({xlBoolean},1);
    sector6=xfix({xlBoolean},0);
    z=xfix({xlUnsigned,10,0},tempv-4*171);
else
    sector1=xfix({xlBoolean},0);
```

```

sector2=xfix({xlBoolean},0);
sector3=xfix({xlBoolean},0);
sector4=xfix({xlBoolean},0);
sector5=xfix({xlBoolean},0);
sector6=xfix({xlBoolean},1);
z=xfix({xlUnsigned,10,0},tempv-5*171);
end

```

ramp2mod.m

```

function z = ramp2(x)
gain=xfix({xlSigned,20,19},1/1800)
z=xfix({xlSigned,14,13},x*gain);

```

thetaconv2.m

```

function [y] = thetaconv(x)
gain1 = xfix({xlSigned,14,10},2*3.14);
gain2 = xfix({xlSigned,14,10},1/gain1)
if x<0
y=xfix({xlUnsigned,10,0},(x+gain1)*gain2*1024);
else
y=xfix({xlUnsigned,10,0},x*gain2*1024);
end

```


C. MATLAB M-FILES FOR CHIPSCOPE INTERFACE

Black_box_dc_machine2_config.m

```
function code_config(this_block)

    % Revision History:
    %
    % 18-Dec-2008 (15:15 hours):
    %     Original code was machine generated by Xilinx's System
Generator
    %     after parsing H:\Docs\work_files\Docs\classes\EC3130_2009\DC
    %     machine lab\black_box_dc_machine2.vhd

    this_block.setTopLevelLanguage('VHDL');

    this_block.setEntityName('code');

    % System Generator has to assume that your entity has a
combinational
    % feed through;
    % if it doesn't, then comment out the following line:
    this_block.tagAsCombinational;

    this_block.addSimulinkInport('ind');
    this_block.addSimulinkInport('ila_clock');
    this_block.addSimulinkInport('ind2');

    this_block.addSimulinkOutport('outd');
    this_block.addSimulinkOutport('open_loop');
    this_block.addSimulinkOutport('speed');

    outd_port = this_block.port('outd');
    outd_port.setType('UFix_1_0');
    open_loop_port = this_block.port('open_loop');
    open_loop_port.setType('UFix_1_0');
    speed_port = this_block.port('speed');
    speed_port.setType('UFix_8_0');

    % -----
    if (this_block.inputTypesKnown)
        % do input type checking, dynamic output type and generic setup in
% this code block.

        if (this_block.port('ind').width ~= 1);
            this_block.setError('Input data type for port "ind" must have
width=1.');
```

```
        end

        this_block.port('ind').useHDLVector(false);
```

```

    if (this_block.port('ila_clock').width ~= 1);
        this_block.setError('Input data type for port "ila_clock" must
have width=1.');
```

end

```

    this_block.port('ila_clock').useHDLVector(false);

    if (this_block.port('ind2').width ~= 48);
        this_block.setError('Input data type for port "ind2" must have
width=48.');
```

end

```

end % if(inputTypesKnown)
% -----

% -----
if (this_block.inputRatesKnown)
    setup_as_single_rate(this_block,'clk','ce')
end % if(inputRatesKnown)
% -----

% Add additional source files as needed.
% |----- | Add files in the order in which they should be
% compiled. | If two files "a.vhd" and "b.vhd" contain the entities
% entity_a and entity_b, and entity_a contains a | component of type
% entity_b, the correct sequence of | addFile() calls would be: |
% this_block.addFile('b.vhd'); | this_block.addFile('a.vhd');
```

|-----

```

%     this_block.addFile(''); this_block.addFile('');
this_block.addFile('black_box_dc_machine2.vhd');
```

return;

% -----

```

function setup_as_single_rate(block,clkname,cename)
inputRates = block.inputRates;
uniqueInputRates = unique(inputRates);
if (length(uniqueInputRates)==1 & uniqueInputRates(1)==Inf)
    block.setError('The inputs to this block cannot all be constant.');
```

return;

```

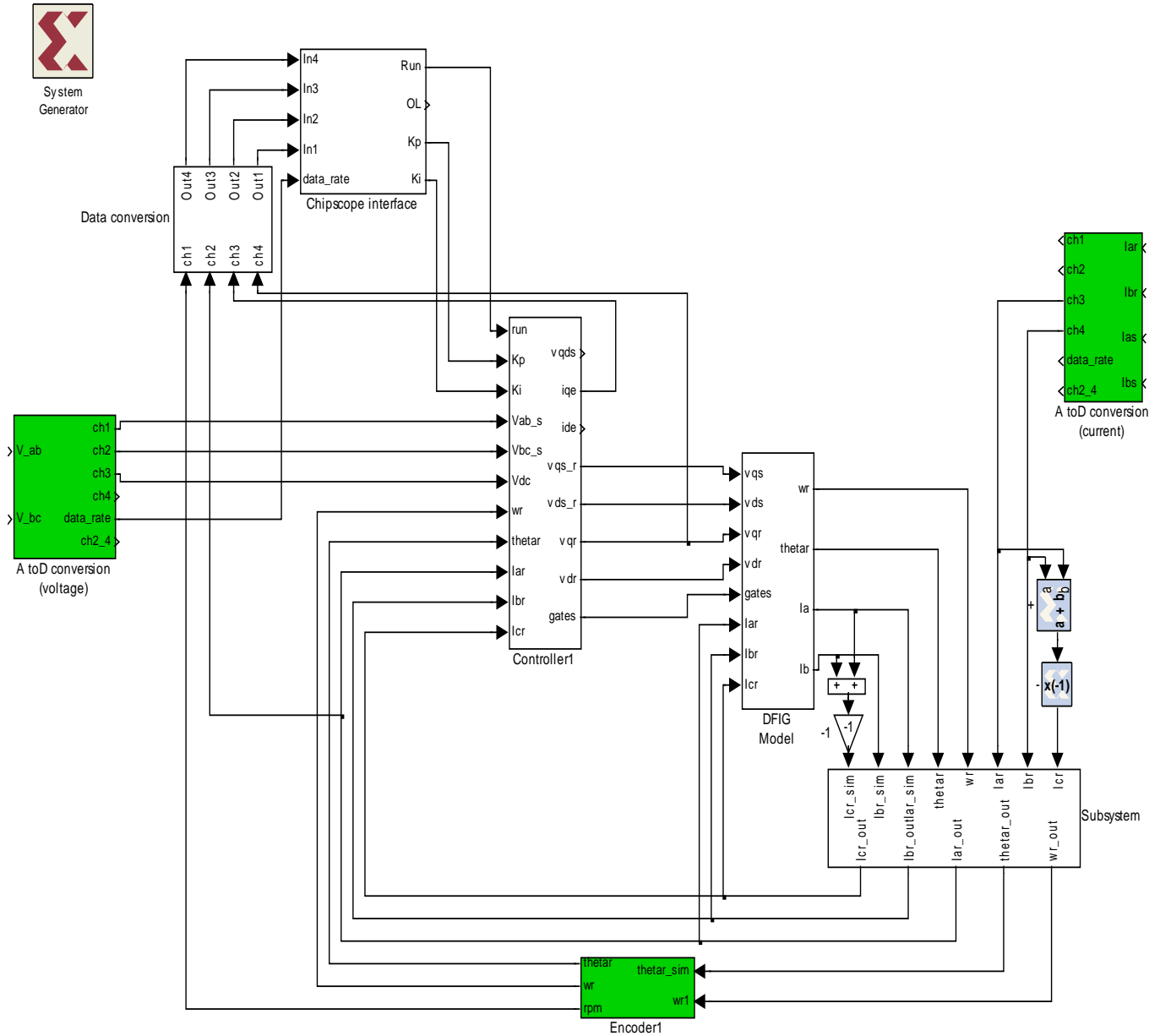
end
if (uniqueInputRates(end) == Inf)
    hasConstantInput = true;
    uniqueInputRates = uniqueInputRates(1:end-1);
end
if (length(uniqueInputRates) ~= 1)
```

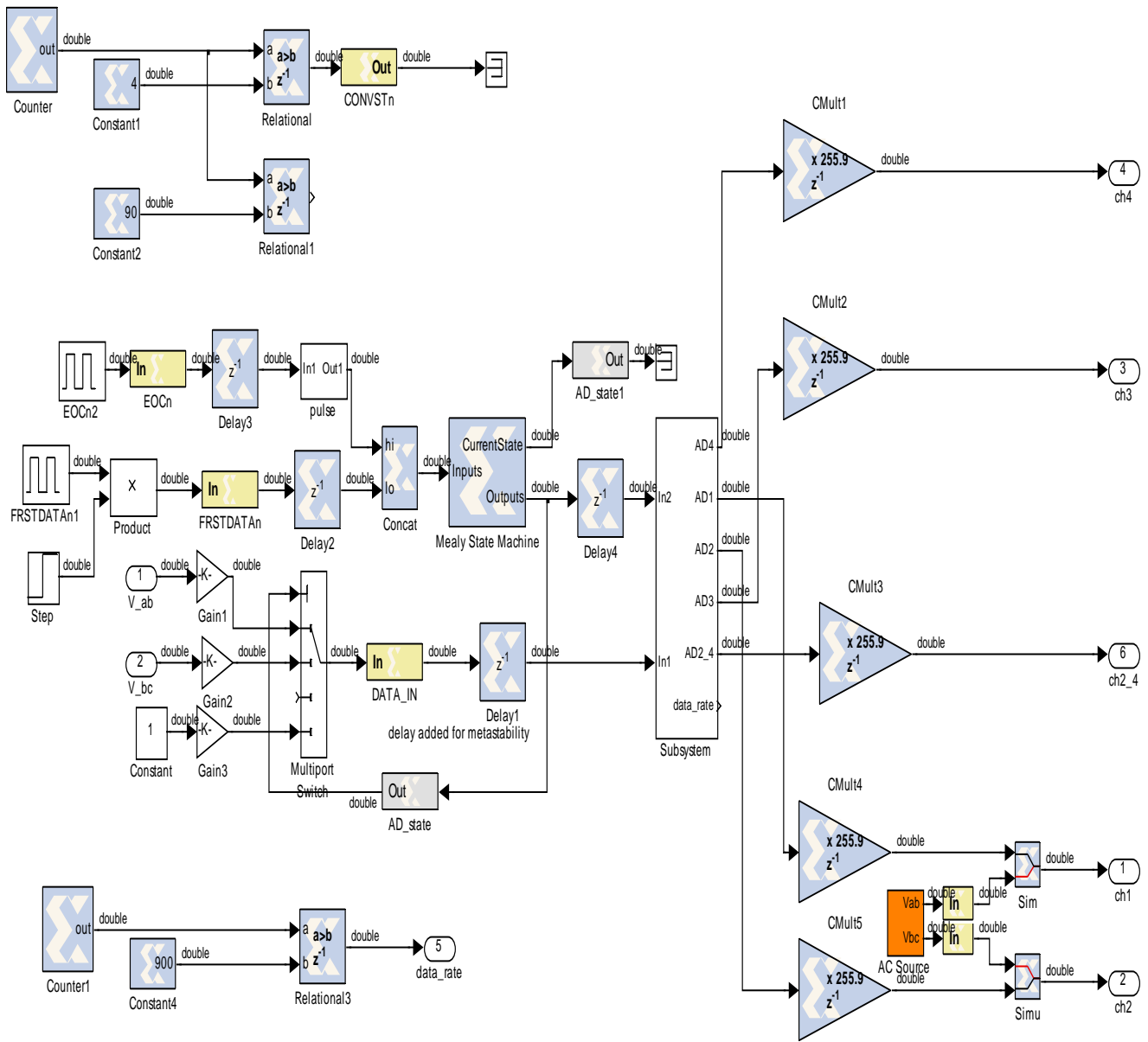
```
    block.setError('The inputs to this block must run at a single
rate.');
```

```
    return;
end
theInputRate = uniqueInputRates(1);
for i = 1:block.numSimulinkOutports
    block.outport(i).setRate(theInputRate);
end
block.addClkCEPair(clkname,cename,theInputRate);
return;

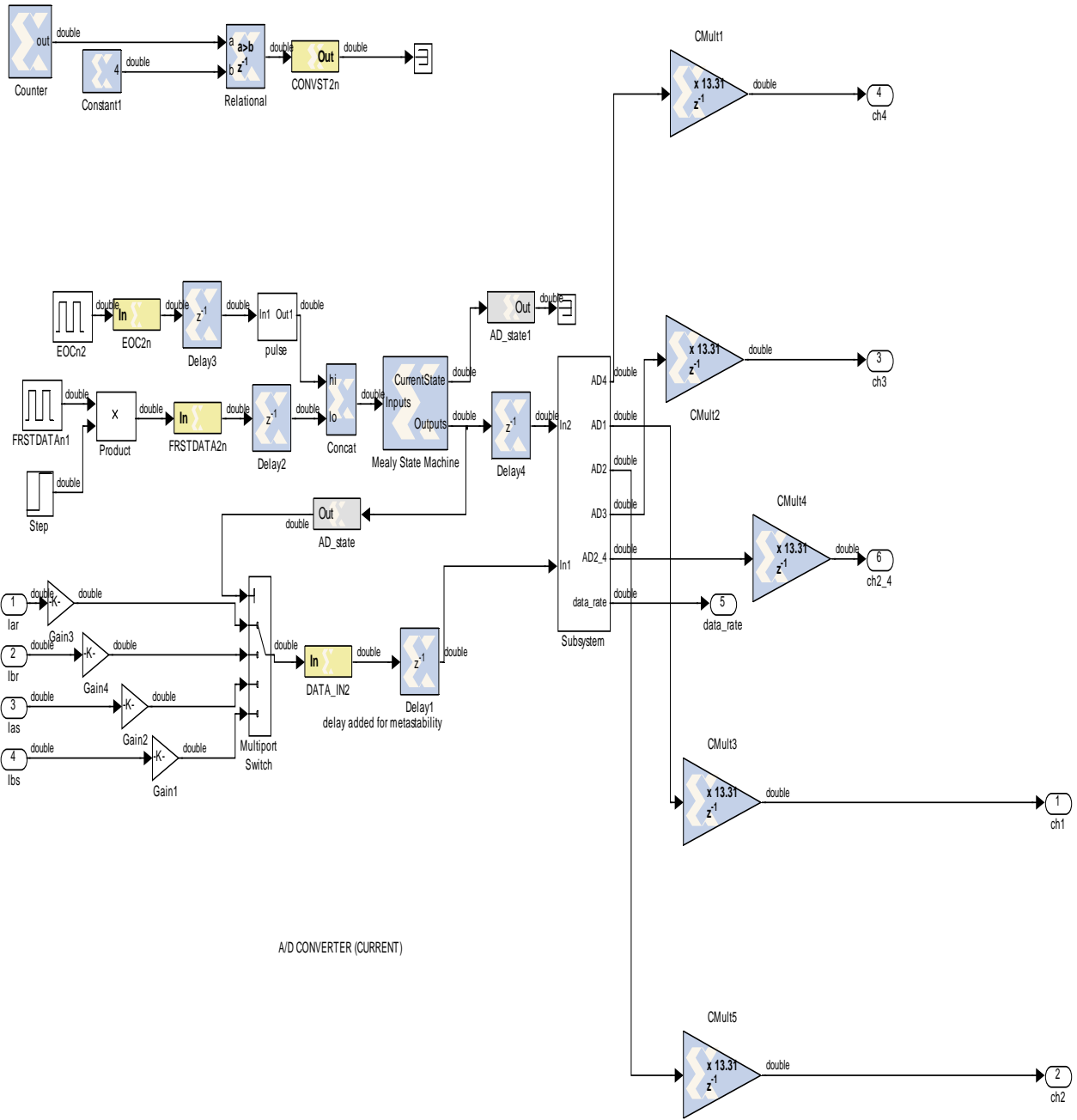
% -----
```

APPENDIX C: SIMULINK/ XILINX MODEL OF WIND TURBINE GENERATOR SYSTEM (DFIG-SIDE)

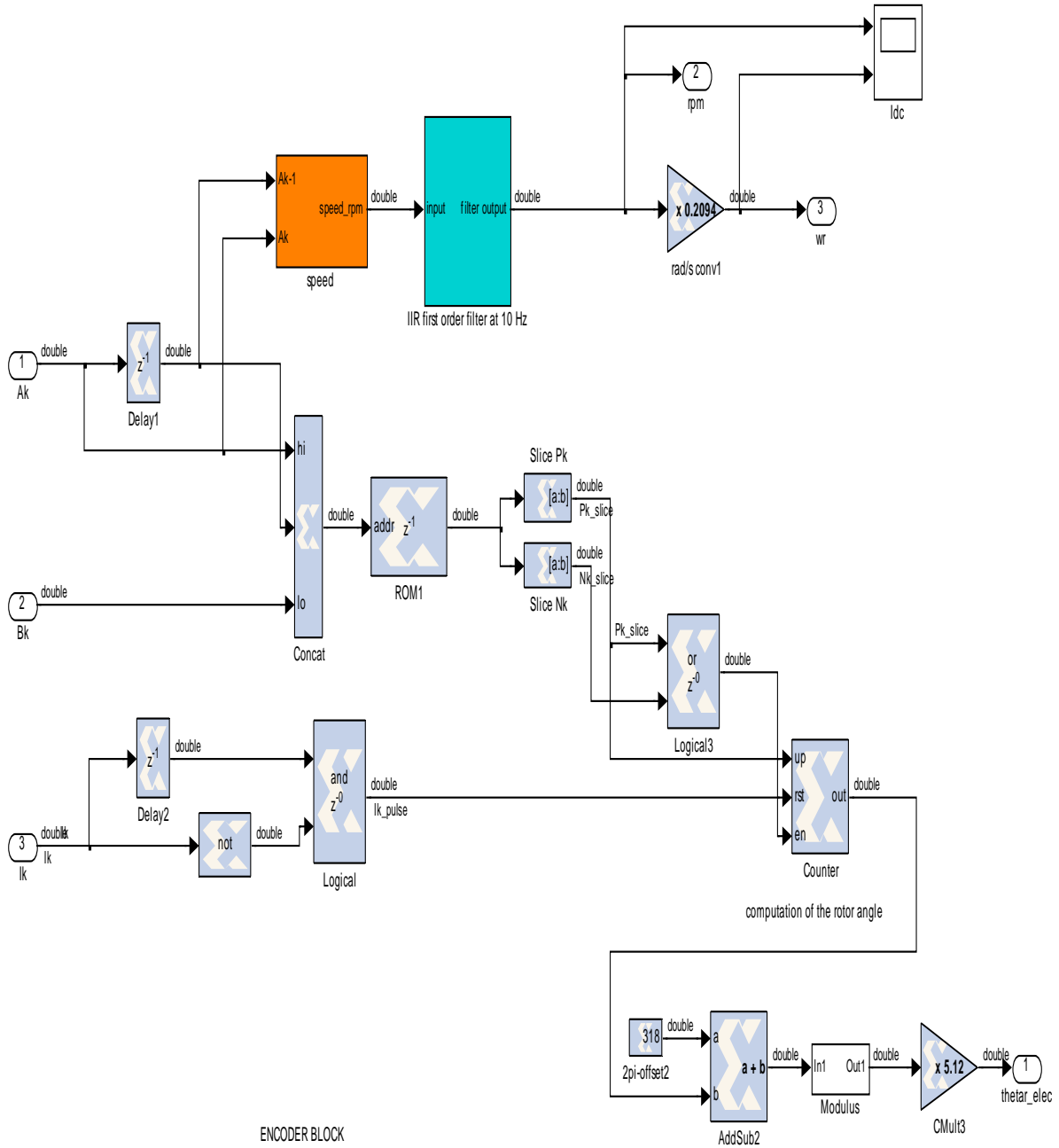




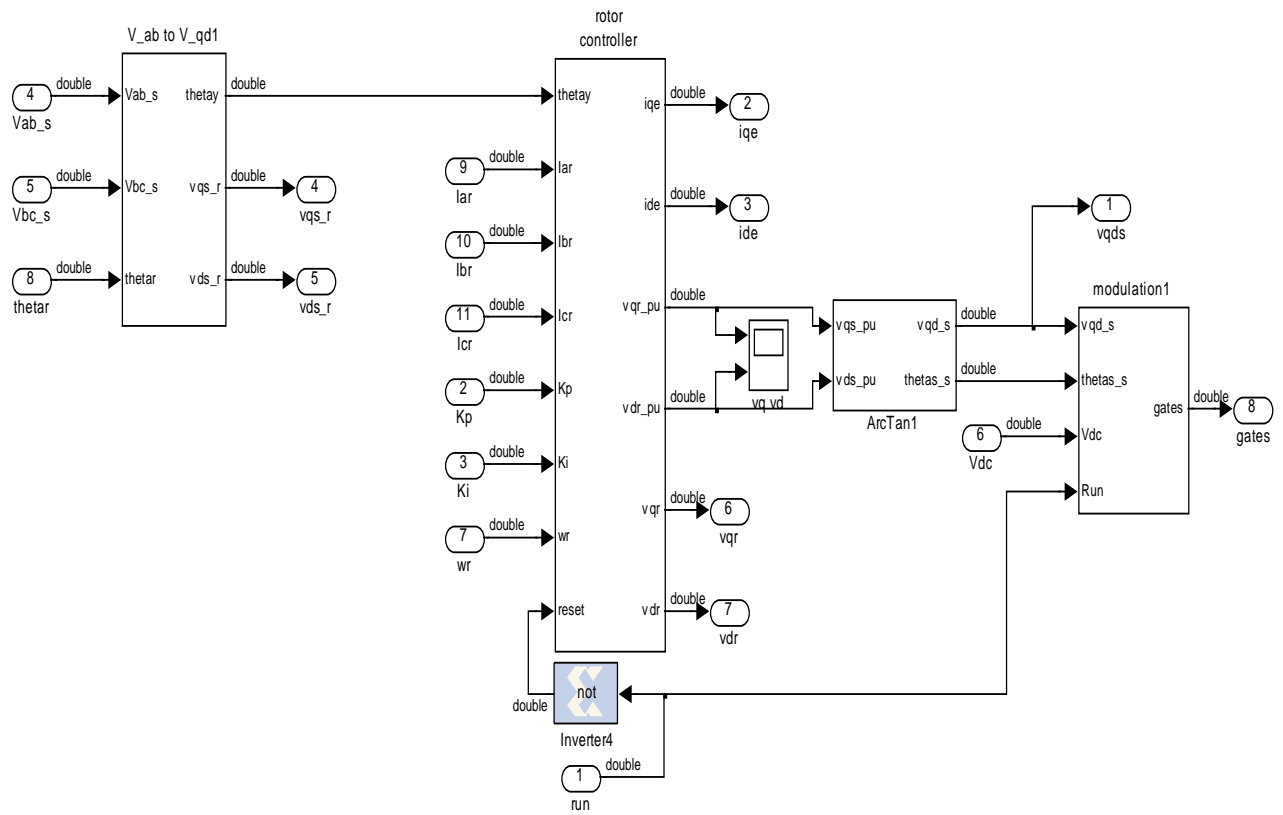
A/D CONVERTER (VOLTAGE)



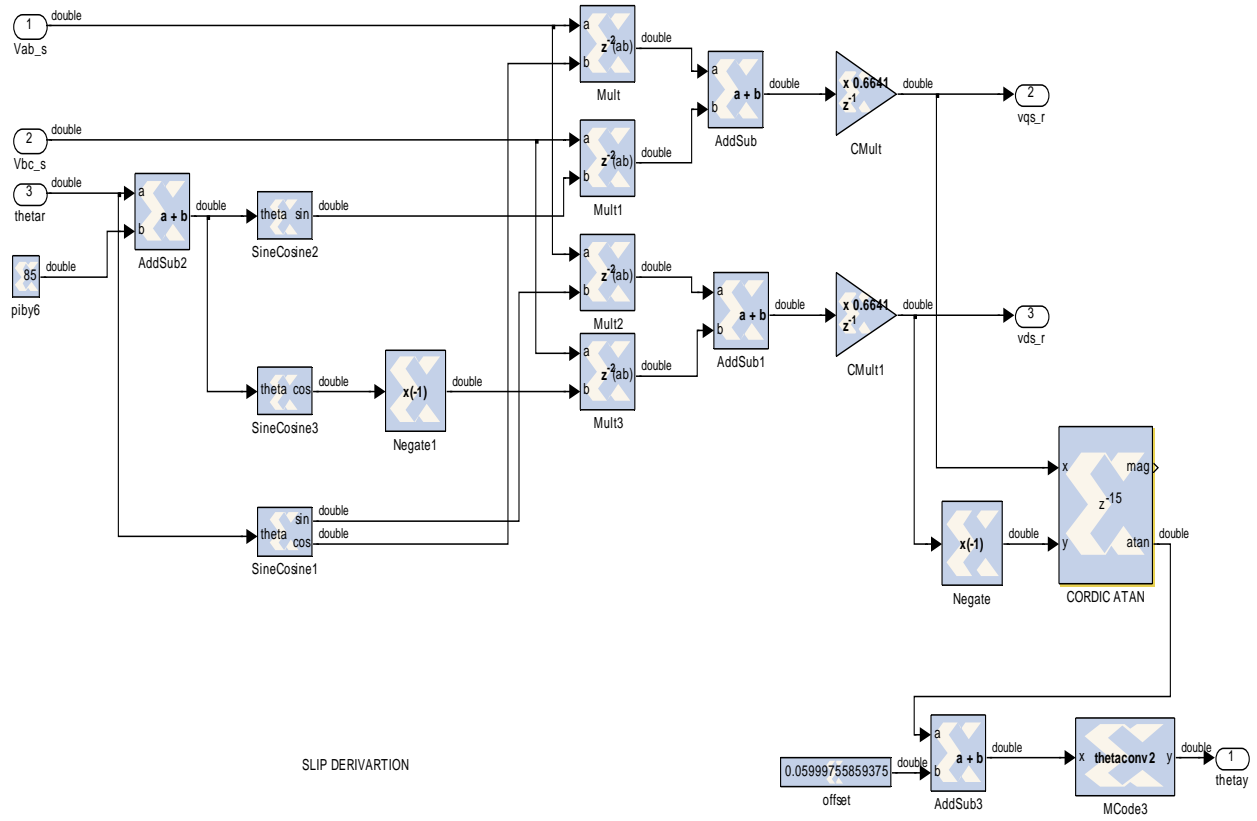
Positive (Pk) and Negative (Nk) bits are created based on Ak transitions and Bk



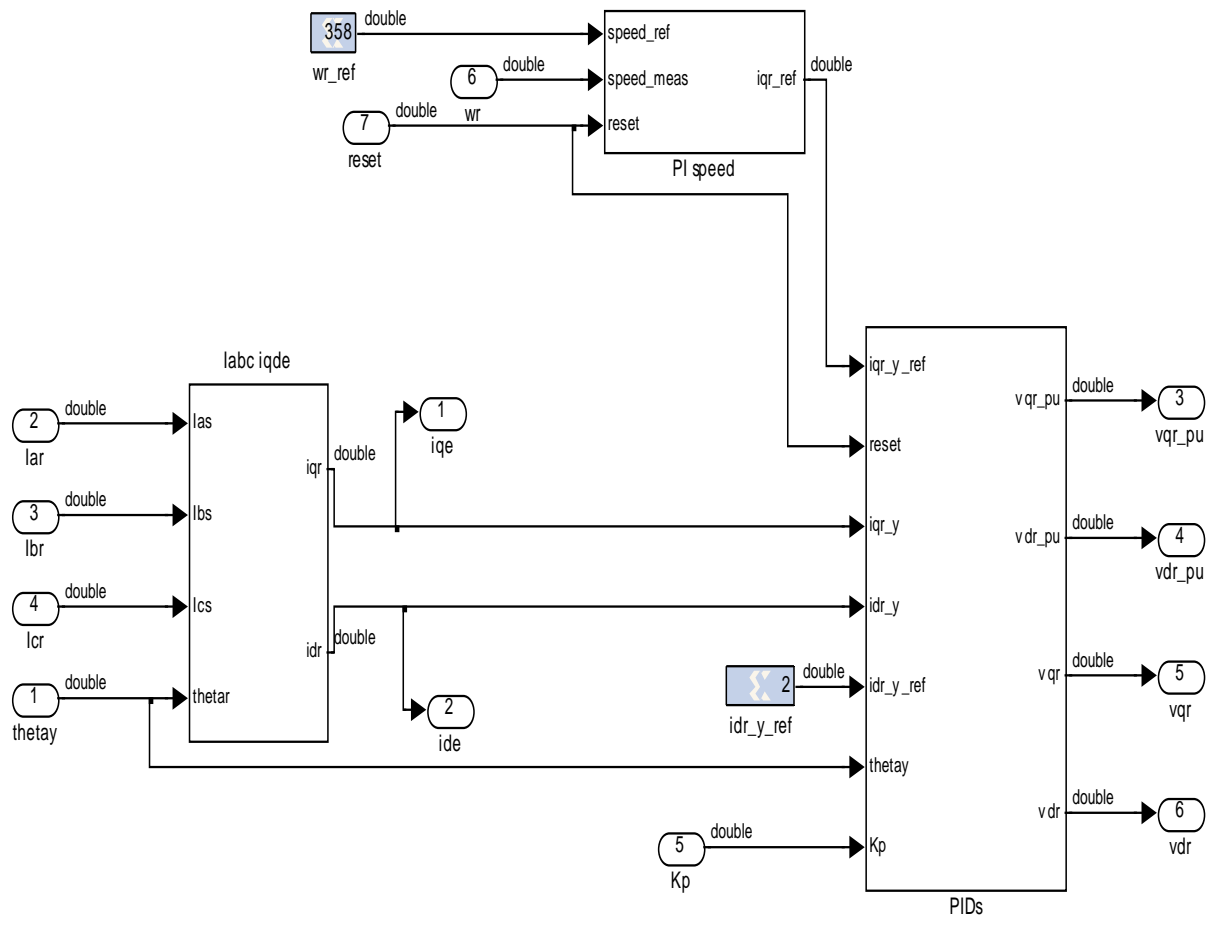
ENCODER BLOCK



ROTOR CONTROLLER



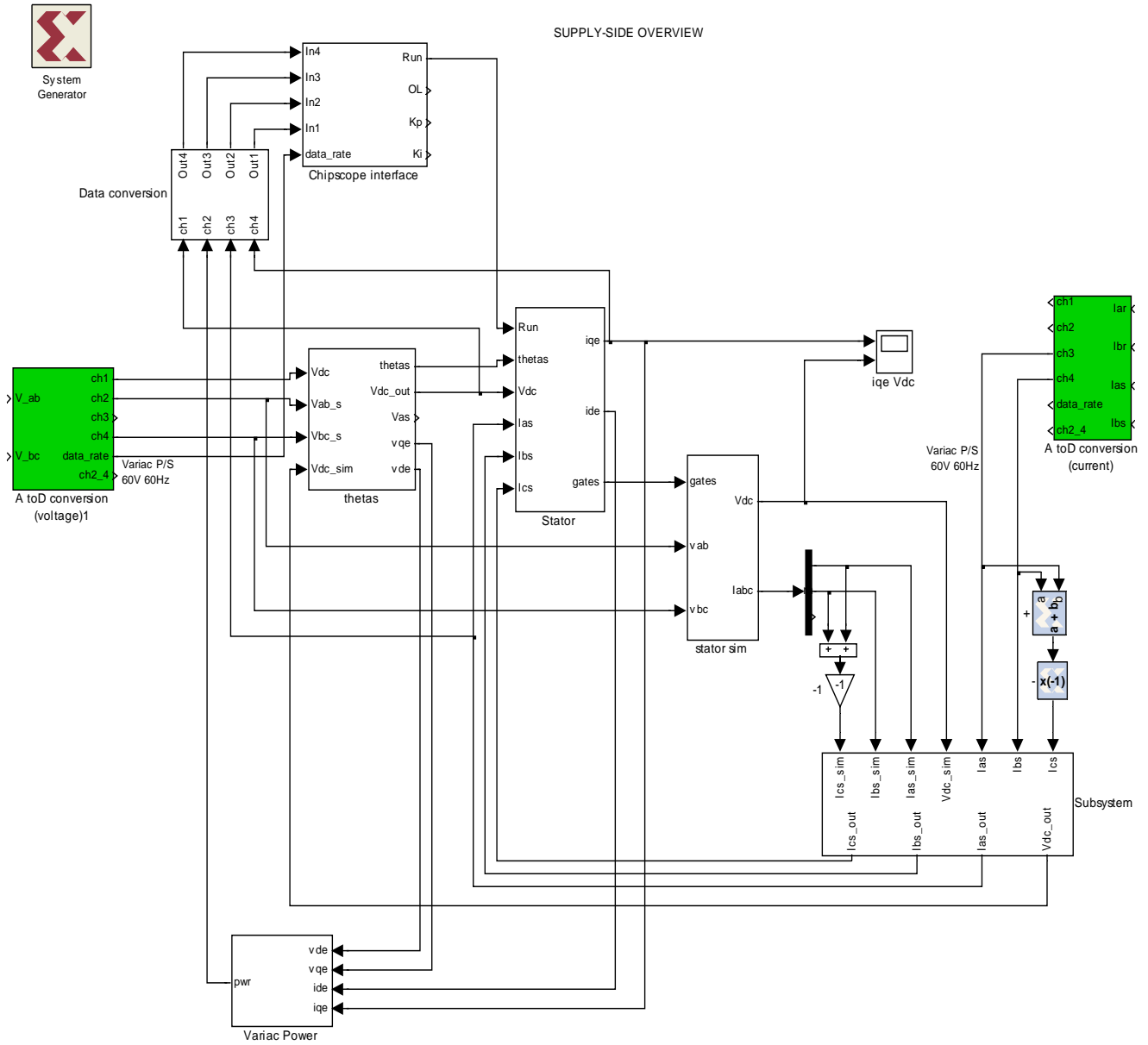
SLIP DERIVATION



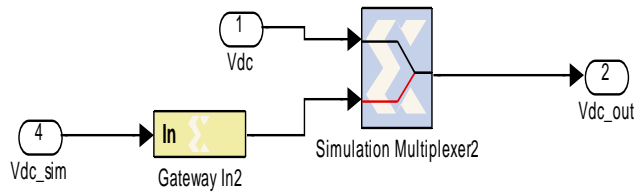
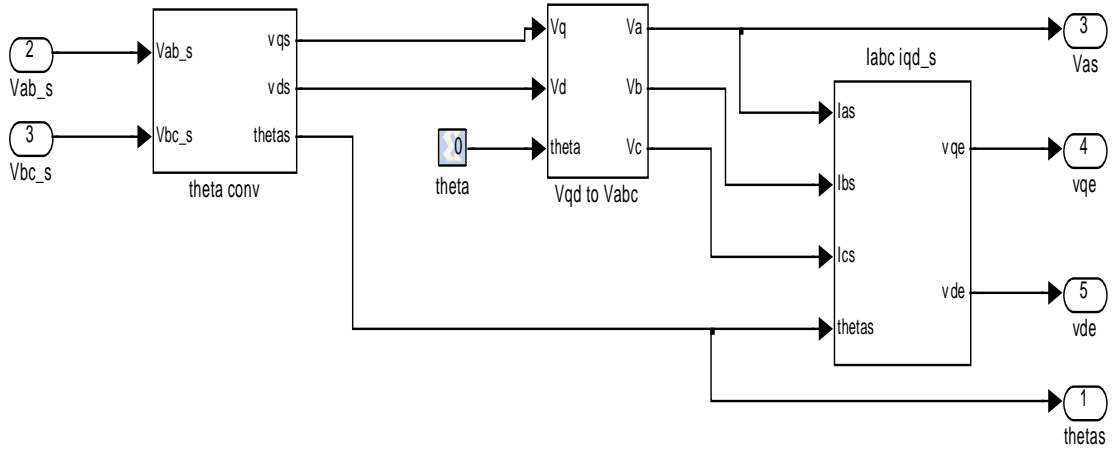
labc to iqde
 SPEED PI
 CURRENT PIs

THIS PAGE INTENTIONALLY LEFT BLANK

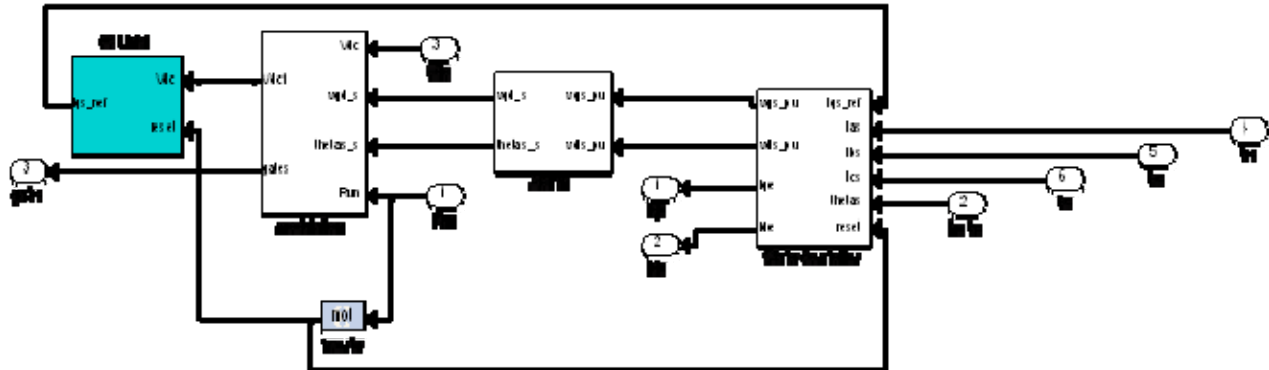
APPENDIX D: SIMULINK/ XILINX MODEL OF WIND TURBINE GENERATOR SYSTEM (SUPPLY-SIDE)



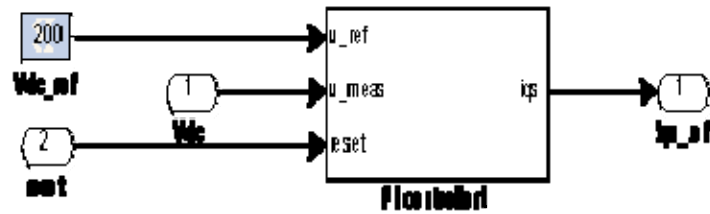
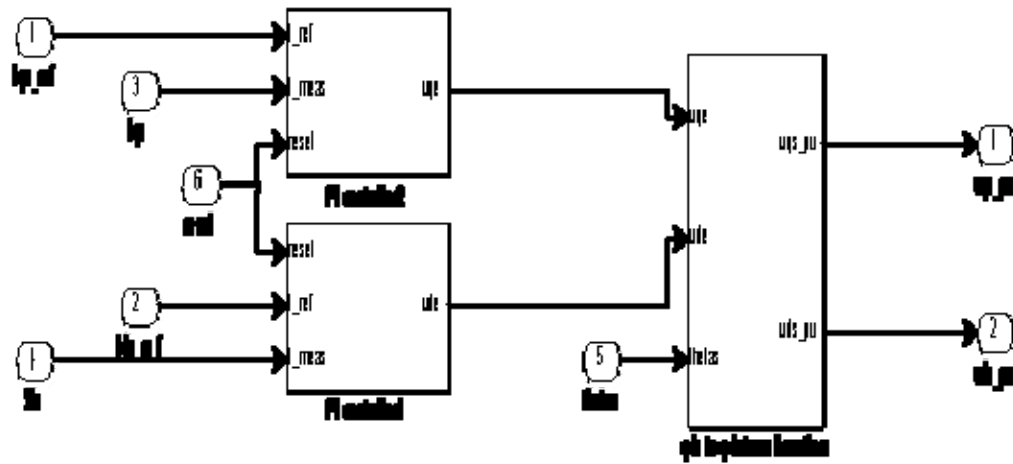
Vabc_s THETA CALCULATION



SUPPLY-SIDE CONTROLLER



PI CONTROLLERS WITH PER-UNIT OUTPUT TO MODULATION



THIS PAGE INTENTIONALLY LEFT BLANK

APPENDIX E: TRANSFORMATIONS

$v_{ab} = v_a - v_b; v_{bc} = v_b - v_c = v_b - (-v_a - v_b)$; where $v_a + v_b + v_c = 0$ for a wye connected capacitor bank (with the neutral floating)

Note also that $i_a + i_b + i_c = 0$ for a wye connected transformer winding set.

$$\begin{bmatrix} v_{ab} \\ v_{bc} \end{bmatrix} = \begin{bmatrix} 1 & -1 \\ 1 & 2 \end{bmatrix} \begin{bmatrix} v_a \\ v_b \end{bmatrix} \Rightarrow \begin{bmatrix} v_a \\ v_b \end{bmatrix} = \frac{1}{3} \begin{bmatrix} 2 & 1 \\ -1 & 1 \end{bmatrix} \begin{bmatrix} v_{ab} \\ v_{bc} \end{bmatrix}$$

$$v_q = \frac{2}{\sqrt{3}} \left[v_a \cos(\theta) + v_b \cos(\theta - 2\pi/3) + v_c \cos(\theta + 2\pi/3) \right]; \text{ ref. Krause text}$$

$$= \frac{2}{\sqrt{3}} \left[v_a \cos(\theta) + v_b \cos(\theta - 2\pi/3) + (-v_a - v_b) \cos(\theta + 2\pi/3) \right]$$

$$= \frac{2}{\sqrt{3}} \left[v_a (\cos(\theta) - \cos(\theta + 2\pi/3)) + v_b (\cos(\theta - 2\pi/3) - \cos(\theta + 2\pi/3)) \right] = \frac{2}{\sqrt{3}} (v_a \sin(\theta + \pi/3) + v_b \sin(\theta))$$

$$v_d = \frac{2}{\sqrt{3}} \left[v_a \sin(\theta) + v_b \sin(\theta - 2\pi/3) + v_c \sin(\theta + 2\pi/3) \right]; \text{ ref. Krause text}$$

$$= \frac{2}{\sqrt{3}} \left[v_a \sin(\theta) + v_b \sin(\theta - 2\pi/3) + (-v_a - v_b) \sin(\theta + 2\pi/3) \right]$$

$$= \frac{2}{\sqrt{3}} \left[v_a (\sin(\theta) - \sin(\theta + 2\pi/3)) + v_b (\sin(\theta - 2\pi/3) - \sin(\theta + 2\pi/3)) \right] = \frac{2}{\sqrt{3}} (-v_a \cos(\theta + \pi/3) - v_b \cos(\theta))$$

$$\begin{bmatrix} v_q \\ v_d \end{bmatrix} = \frac{2}{\sqrt{3}} \begin{bmatrix} \sin(\theta_e + \pi/3) & \sin(\theta_e) \\ -\cos(\theta_e + \pi/3) & -\cos(\theta_e) \end{bmatrix} \frac{1}{3} \begin{bmatrix} 2 & 1 \\ -1 & 1 \end{bmatrix} \begin{bmatrix} v_{ab} \\ v_{bc} \end{bmatrix} = \frac{2}{3\sqrt{3}} \begin{bmatrix} \sin(\theta_e + \pi/3) & \sin(\theta_e) \\ -\cos(\theta_e + \pi/3) & -\cos(\theta_e) \end{bmatrix} \begin{bmatrix} 2 & 1 \\ -1 & 1 \end{bmatrix} \begin{bmatrix} v_{ab} \\ v_{bc} \end{bmatrix}$$

$$\begin{bmatrix} v_q \\ v_d \end{bmatrix} = \frac{2}{\sqrt{3}} \begin{bmatrix} \cos(\theta_e) & \sin(\theta_e + \pi/6) \\ \sin(\theta_e) & -\cos(\theta_e + \pi/6) \end{bmatrix} \begin{bmatrix} v_{ab} \\ v_{bc} \end{bmatrix}; \text{ transformation used for measured line-to-line voltages}$$

THIS PAGE INTENTIONALLY LEFT BLANK

LIST OF REFERENCES

- [1] R. Pena, J. C. Clare, and G. M. Asher, "Doubly fed induction generator using back-to-back PWM converters and its application to variable speed wind-energy generation," IEE Proc.-Electr. Power Appl., Vol.143, No 3, May 1996.
- [2] Shuhui Li and Timothy A. Haskew, "Analysis of Decoupled d-q Vector Control in DFIG Back-to-Back PWM Converter," Power Engineering Society General Meeting, 2007, IEEE, 24-28 June 2007, pp.1-7.
- [3] G.A. Smith and K.A. Nigim, "Wind-energy recovery by a static Scherbius induction generator," IEE Proc., Vol.128, Pt. C, No 6, November 1981.
- [4] Jason G. Massey, "Doubly Fed Induction Machine Control For Wind Energy Conservation," Master's Thesis, Naval Postgraduate School, 2009.
- [5] H.N. Robey, H.O. Stevens and K.T. Page, "Application of Variable Speed Constant Frequency Generators to Propulsion-Derived Ship Service," Naval Engineers Journal, May 1985; pp.296-305.
- [6] Joseph E. O'Conner, "Field Programmable Gate Array Control of Power Systems in Graduate Student Laboratories," Master's Thesis, Naval Postgraduate School, 2008.
- [7] Paul C. Krause, Oleg Wasynczuk, and Scott D. Sudhoff. "Analysis of Electric Machinery and Drive Systems," John Wiley & Sons, 2002.
- [8] Alexander Julian, Giovanna Oriti, "FPGA Based Digital Implementation of Naturally Sampled Space Vector Modulation," ECCE 2009, to be presented, 20-24 Sep 2009.
- [9] Alexander. L. Julian, Notes for EC4130 (Advanced Electrical machinery Systems), Naval Postgraduate School, 2007 (unpublished).
- [10] Andrew M. La Valley, "Design and Implementation of a Motor Incremental Shaft Encoder," Master's Thesis, Naval Postgraduate School, 2008.

THIS PAGE INTENTIONALLY LEFT BLANK

INITIAL DISTRIBUTION LIST

1. Defense Technical Information Center
Ft. Belvoir, Virginia
2. Dudley Knox Library
Naval Postgraduate School
Monterey, California
3. Dr. Jeffrey Knorr
Electrical Engineering and Computer Department
Code EC/Ko
Naval Postgraduate School
Monterey, California
4. Dr. Alexander Julian
Electrical Engineering and Computer Department
Code EC/J1
Naval Postgraduate School
Monterey, California
5. Dr. Roberto Cristi
Electrical Engineering and Computer Department
Code EC/C1
Naval Postgraduate School
Monterey, California
6. Capt. Lynn J. Petersen USN
Oxford, Pennsylvania
7. Steven B. Swindler, PE
Naval Surface Warfare Center
Carderock Division Code 9820
West Bethesda, Maryland
8. Joe Borricinni
NAVSEA PHL Code 9820
Philadelphia, Pennsylvania